Wind Speed as a Dominant Source of Periodicities in Reported Emission Rates of Volcanic SO 2

C. Barrington, B. Taisne, F. Costa, S. Arellano

▶ **To cite this version:**

C. Barrington, B. Taisne, F. Costa, S. Arellano. Wind Speed as a Dominant Source of Periodicities in Reported Emission Rates of Volcanic SO 2. Journal of Geophysical Research : Solid Earth, 2022, 127 (12), ⟨10.1029/2022jb025380⟩. ⟨hal-03953738⟩

HAL Id: hal-03953738

https://hal.science/hal-03953738v1

Submitted on 24 Jan 2023

HAL is a multi-disciplinary open access archive for the deposit and dissemination of scientific research documents, whether they are published or not. The documents may come from teaching and research institutions in France or abroad, or from public or private research centers.

L'archive ouverte pluridisciplinaire **HAL**, est destinée au dépôt et à la diffusion de documents scientifiques de niveau recherche, publiés ou non, émanant des établissements d'enseignement et de recherche français ou étrangers, des laboratoires publics ou privés.

HAL Authorization

Check for updates

JGR Solid Earth

RESEARCH ARTICLE
10.1029/2022JB025380

Wind Speed as a Dominant Source of Periodicities in Reported Emission Rates of Volcanic SO_2

C. Barrington[1,2], B. Taisne[1,2], F. Costa[1,2,3], and S. Arellano[4]

[1]Earth Observatory of Singapore and Nanyang Technological University, Singapore, [2]Asian School of the Environment, Nanyang Technological University, Singapore, [3]Institut de Physique du Globe de Paris, Université Paris Cité, CNRS, Paris, France, [4]Department of Space, Earth and Environment, Chalmers University of Technology, Gothenburg, Sweden

Key Points:

- Majority of periodicities identified in the emission rate of SO_2 are related global trade winds and not volcanic in origin
- We identified periodicities between 30 and 70 days that are associated to the Madden-Julian Oscillation
- We find no statistically significant periodicities related to the long-term influence of Earth tides on volcanic degassing of SO_2

Correspondence to:

C. Barrington,
charlott001@e.ntu.edu.sg

Citation:

Barrington, C., Taisne, B., Costa, F., & Arellano, S. (2022). Wind speed as a dominant source of periodicities in reported emission rates of volcanic SO_2. *Journal of Geophysical Research: Solid Earth*, *127*, e2022JB025380. https://doi.org/10.1029/2022JB025380

Received 9 AUG 2022
Accepted 4 DEC 2022

Author Contributions:

Conceptualization: C. Barrington, B. Taisne, F. Costa, S. Arellano
Formal analysis: C. Barrington, B. Taisne, F. Costa
Software: C. Barrington, B. Taisne
Writing – original draft: C. Barrington, F. Costa
Writing – review & editing: B. Taisne, F. Costa, S. Arellano

© 2022. The Authors.
This is an open access article under the terms of the Creative Commons Attribution License, which permits use, distribution and reproduction in any medium, provided the original work is properly cited.

Abstract Volcanoes have been found to display periodicities or cyclic trends in a wide range of phenomena. These include the eruptive activity itself, but also in the time series of geophysical and geochemical monitoring data such as volcanic degassing. Here, we test the existence of periodicities of volcanic degassing at 32 volcanoes using the time series of sulfur dioxide (SO_2) emission rates from data of the Network of Volcanic and Atmospheric Change (NOVAC). We use the Lomb-Scargle periodogram to analyze the SO_2 data which allows efficient computation of a Fourier-like power spectrum from unevenly sampled data. We were able to calculate False-Alarm Probabilities in 28 of the 32 volcanoes, and we identified significant periodicities in the SO_2 emission rates in 17 of the 28 volcanoes. However, we find that most of these periodicities are also present in the plume speeds used to determine SO_2 emission rates. Periodicities at about 30–70, ~120, and ~180 days were identified at volcanoes located between 16°N and 16°S and are related to intraseasonality and interseasonality in global trade winds and not volcanic in origin. Periodicities between 30 and 70 days in both plume speed and SO_2 emission rates are associated to the Madden-Julian Oscillation that is responsible for intraseasonal variability in the tropical atmosphere. Our study highlights the importance of using local wind data for deriving realistic SO_2 emissions and the identification of short-term periodicity in volcanic behavior.

Plain Language Summary Volcanoes may show cycling patterns in their eruption patterns but also in the geophysical and geochemical data used to monitor them. When these patterns occur at fixed-time intervals, volcanic behavior may be described as periodic. Periodic patterns in volcanic phenomena may reveal the existence of a fundamental process which regulates the inner workings of the volcano and ultimately aid forecasts of eruptive activity. We analyzed the sulfur dioxide degassing patterns of 32 volcanoes from a global database and we reveal significant periodic patterns in 17 of them. However, we also find similar periodic patterns the wind speed of the volcanic plume. We propose that periodic patterns in the degassing rates do not represent physical-chemical processes inside the volcano but result from atmospheric dynamics.

1. Introduction

The identification of periodicities in volcanic phenomena could help to understand the underlying physio-chemical processes that produce them and thus better anticipate volcanic behavior. Periodicity of volcanic activity was probably first proposed for the 1872 eruption of Vesuvius (Italy) where the occurrence of lava flows appeared to coincide with the full moon (Palmieri, 1873). This hypothesis sparked similar observations throughout the 20th century which fed a growing theory for the influence of tidal forces on volcanism (Jaggar et al., 1924; Johnson & Mauk, 1972; Michael & Christoffel, 1975). As more sophisticated monitoring networks were implemented during the 21st century, evidence for periodic behavior has been documented in the instrumental record at several volcanoes (e.g., Conde et al., 2014; Girona et al., 2018; Lamb et al., 2014). Recent advancements in our ability to study volcanic gas emissions have served to renew focus on the role of Earth tides on volcanic activity as well as highlight the extent to which periodic or cyclic trends, in general, have been observed (Bredemeyer & Hansteen, 2014; Dinger et al., 2018; Pering et al., 2019; Figure 1).

Periodicity and cyclicity are typically used synonymously in volcanology, despite having different implications. Here, we refer to periodicity as an event or trend which is regularly recurrent. This includes the tendency for eruptions to occur at well-defined time intervals, in addition to cycles that occur in geophysical or geochemical time series which are systematic over time. Cyclicity is often interpreted as episodes of magma replenishment and ascent, and may be used to aid interpretations of monitoring data for the purpose of forecasting volcanic activity

21699356, 2022, 12, Downloaded from https://agupubs.onlinelibrary.wiley.com/doi/10.1029/2022JB025380 by Cochrane France, Wiley Online Library on [05/01/2023]. See the Terms and Conditions (https://onlinelibrary.wiley.com/terms-and-conditions) on Wiley Online Library for rules of use; OA articles are governed by the applicable Creative Commons License

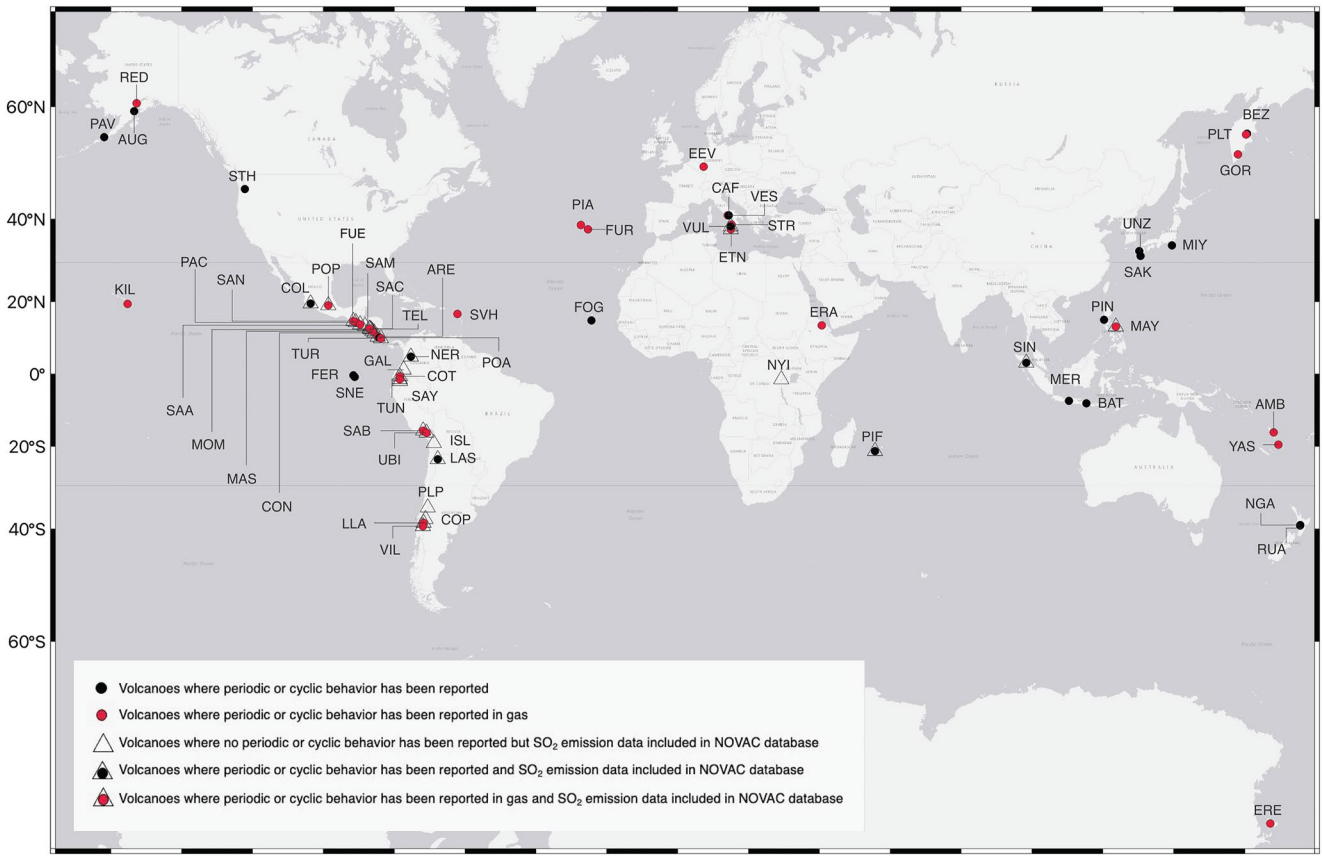

Figure 1. Geographical location of volcanoes where periodic or cyclic trends have been observed. We consider peer-reviewed journal publications and books, whereby the authors use cyclic or periodic to describe volcanic activity or, trends in observational, geophysical, or geochemical time series data which have been linked to the volcanic system or its external modulation. We discriminate between cyclic behavior which implies repeated patterns and cycle which is often used to distinguish different episodes of activity (e.g., Borgia & van Wyk de Vries, 2003) and exclude studies which correlate the timing of a single eruption to known periodic phenomena in nature (e.g., Ebisuzaki et al., 2011; Machado, 1967). We have considered all types of data, including, but not limited to visual observations, seismicity, deformation; volcanic activity inferred from mapped deposits; satellite observations, direct sampling, and ground-based remote sensing of volcanic gases. For each volcano, the first study (or studies, if published in the same volume) reporting cyclic or periodic trends has been cited. Where such trends have also been identified in volcanic-gas data or thought to represent volcanic degassing (inferred from geophysical time series), the first study reporting cyclic or periodic trends in volcanic degassing has also been cited. The following studies have contributed to this figure: AMB: Ambrym, Vanuatu (Allard et al., 2016); ARE: Arenal, Costa Rica (Melson & Saenz, 1973; Williams-Jones et al., 2001); AUG: Augustine, USA (Mauk & Kienle, 1973); BAT: Batur, Indonesia (Neuberg, 2000); BEZ: Bezymianny Russia (Belousov et al., 2002); CAF: Campi Flegrei, Italy (Granieri et al., 2003); COL: Fuego de Colima, Mexico (Luhr & Carmichael, 1980); COT: Cotopaxi, Ecuador (Dinger et al., 2018); EEV: East Eifel Volcanic Field, Germany (Berberich et al., 2019); ERE: Erebus, Antarctica (Sweeney et al., 2008); ERA: Erta Ale, Ethiopia (Bouche et al., 2010); ETN: Etna, Italy (Sottili et al., 2007; Tamburello et al., 2013); FER: Fernandina, Ecuador (Filson et al., 1973); FOG: Fogo, Cape Verde (Custodio et al., 2003); FUE: Fuego, Guatemala (Lyons et al., 2010; Pering et al., 2019 data taken from Nadeau et al. (2011)); FUR: Furnas, Portugal (Viveiros et al., 2015); GOR: Gorely, Russia (Pering et al., 2019 data taken from Aiuppa et al. (2012)); KIL: Kilauea, USA (Connor et al., 1988; Jaggar et al., 1924); LAS: Lascar, Chile (Matthews et al., 1997); LLA: Llaima, Chile (Bredemeyer & Hansteen, 2014); MAS: Masaya, Nicaragua (Stoiber et al., 1986); MAY: Mayon, Philippines (Girona et al., 2018; Ramos et al., 1985); MER: Merapi, Indonesia (Fadeli et al., 1991); MIY: Miyakejima, Japan (Kasahara et al., 2001); NER: Nevado del Ruiz, Colombia (Martinelli, 1990); NGA: Ngauruhoe, New Zealand (Michael & Christoffel, 1975); PAC: Pacaya, Guatemala (Battaglia et al., 2018); PAV: Pavlof (McNutt & Beavan, 1981); PIA: Pico Alto (Aumento, 2002); PIN: Pinatubo, Philippines (Mori et al., 1996); PIF: Piton de la Fournaise, France (Peltier et al., 2008); PLT: Plosky Tolbachik, Russia (Telling et al., 2015); POA: Poás, Costa Rica (Rymer, 2005); POP: Popocatépetl, Mexico (Campion et al., 2018); RED: Redoubt, USA (Lopez et al., 2013); RUA: Ruapehu, New Zealand (Girona et al., 2018); SAB: Sabancaya, Peru (Moussallam et al., 2017); SAK: Sakurajima, Japan (Yokoo et al., 2013); SAC: San Cristóbal, Nicaragua (Conde et al., 2016); SAA: Santa Ana, El Salvador (Bernard et al., 2004; Salazar et al., 2004); SAN: Santiaguito, Guatemala (Holland et al., 2011; Rose, 1987); SNE: Sierra Negra, Ecuador (Chadwick et al., 2006); SIN: Sinabung, Indonesia (Nakada et al., 2019); SVH: Soufriere Hill, UK (Edmonds et al., 2003; Voight et al., 1998); STH: St. Helens, USA (McNutt & Beavan, 1984); STR: Stromboli, Italy (Johnson & Mauk, 1972; Ripepe et al., 2002); TUR: Turrialba, Costa Rica (Conde et al., 2014); TUN: Tungurahua, Ecuador (Neuberg et al., 2018; Warnach et al., 2019); UBI: Ubinas, Peru (Moussallam et al., 2017); UNZ: Unzen, Japan (Nakada et al., 1999); VES: Vesuvius, Italy (Palmieri, 1873); VIL: Villarrica, Chile (Bredemeyer & Hansteen, 2014); VUL: Vulcano, Italy (Bottari et al., 1992); and YAS: Yasur, Vanuatu (Bani & Lardy, 2007). We note that this is not intended as an exhaustive list but serves to highlight the prevalence of cyclic and periodic trends at volcanoes globally. Volcanoes excluded from this list, but with SO_2 emissions data made available via the NOVAC Database and considered in this study, are also highlighted: CON: Concepción, Nicaragua; COP: Copahue, Chile-Argentina; GAL: Galeras, Colombia; ISL: Isluga, Chile-Bolivia; MOM: Momotombo, Nicaragua; NYI: Nyiragongo, Democratic Republic of the Congo; PLP: Planchón-Peteroa, Chile; SAY: Sangay, Ecuador; SAM: San Miguel, El Salvador; and TEL: Telica, Nicaragua. Horizontal lines indicate 30°N and 30°S, latitudes within which the trade winds move from east to west on either side of the equator.

21699356, 2022, 12, Downloaded from https://agupubs.onlinelibrary.wiley.com/doi/10.1029/2022JB025380 by Cochrane France, Wiley Online Library on [05/01/2023]. See the Terms and Conditions (https://onlinelibrary.wiley.com/terms-and-conditions) on Wiley Online Library for rules of use; OA articles are governed by the applicable Creative Commons License

21699356, 2022, 12, Downloaded from https://agupubs.onlinelibrary.wiley.com/doi/10.1029/2022JB025380 by Cochrane France, Wiley Online Library on [05/01/2023]. See the Terms and Conditions (https://onlinelibrary.wiley.com/terms-and-conditions) on Wiley Online Library for rules of use; OA articles are governed by the applicable Creative Commons License

(Christopher et al., 2015; Neuberg et al., 2018; Peltier et al., 2008). Where these cycles are periodic, they are thought to represent volcanoes external modulation of, or sensitivity to, processes in nature which operate at the same periodicity (Dinger et al., 2019; Ebisuzaki et al., 2011; Girona et al., 2018) or a fundamental characteristic of the system (Michaut et al., 2013). Periodicities of 50–55 days have been found in monitored parameters at several volcanoes: Fuego de Colima, Mexico (Lamb et al., 2014), Masaya, Nicaragua (Pering et al., 2019), Plosky Tolbachik, Kamchatka (Telling et al., 2015), and Soufriere Hills Volcano (SHV), Montserrat (Christopher et al., 2015) causing speculation that they are due to a process that is common among the volcanoes (e.g., Lamb et al., 2014). While several scenarios have been put forward to account for these observations, the source of the periodicities is not well-established (e.g., Lopez et al., 2013), and it remains unclear whether these periodic trends are discontinuous or permanent features of volcanic activity.

Periodicities in geochemical time series range from about seconds or minutes (Aiuppa et al., 2012; Girona et al., 2015; Tamburello et al., 2013), to several weeks or months (Christopher et al., 2015; Pering et al., 2019). This range in reported periodicities may reflect the behavior and state of the system, but also depends on the instrumental techniques and therefore sampling rate used to study volcanic gases. Periodicities have been observed in time series of diffuse gas emanations of radon (Aumento, 2002; Cigolini et al., 2009) and CO_2 (Viveiros et al., 2015), as well as in the relative concentrations of plume-gas species recorded by electrochemical sensors (Moussallam et al., 2017) and ground-based remote sensing techniques, including Fourier-Transform Infrared (FTIR; Allard et al., 2016) and Differential Optical Absorption Spectroscopy (DOAS; Dinger et al., 2018, 2021; Warnach et al., 2019). The emission rate of SO_2 as a plume-gas is an important parameter for forecasting activity and monitoring ongoing eruptions for the world's most active volcanoes. Periodicities in the time series of SO_2 emission rates have been recorded at several volcanoes, using correlation spectroscopy (Connor et al., 1988; Sweeney et al., 2008), satellite remote sensing (Flower & Carn, 2015; Lopez et al., 2013; Telling et al., 2015), UV cameras (Campion et al., 2018; Tamburello et al., 2013), as well as ground-based UV-spectrometers (Bredemeyer & Hansteen, 2014; Conde et al., 2014). Identification of periodic trends from a range of volcanoes with vastly different characteristics, implies that periodicities are a fundamental component of volcanic plume degassing (Pering et al., 2019) which could provide fundamental insights into the processes controlling volcanic degassing and in turn, aid our ability to forecast eruptions.

Thanks to the development of low-cost UV-spectrometers at the start of the 21st century (Galle et al., 2002), emission rates of SO_2 are now continuously measured at an increasing number of volcanoes. The Network of Volcanic and Atmospheric Change (NOVAC) is the largest instrument network for monitoring volcanic gases globally and comprises a community of volcano observatories and research institutions that apply DOAS to spectra recorded by grounded-based scanning UV-spectrometers (Galle et al., 2010). Data obtained by the NOVAC network have contributed to a large database providing time series of SO_2 emission rates from a total of 32 volcanoes (Arellano et al., 2021). Owing to a strict data selection protocol and standardized methodology, the database provides time series of good quality, daily SO_2 emissions for a range of volcanoes which cover time scales of just a few days to several years, between 2005 and 2017. Access to data from the NOVAC Database provides a novel opportunity to identify periodicities in volcanic SO_2 emissions from volcanoes with different characteristics. Here, we perform an analysis of SO_2 degassing time series data from the NOVAC network to identify possible periodicities and discuss them in the context of their use to understand volcanic systems and methods involved to derive the SO_2 emission rates.

2. Materials and Methods

2.1. Time Series of SO_2 Emission Rate

NOVAC is the largest instrument network for monitoring volcanic gases, with a total of 100 instruments installed across 42 volcanoes (NOVAC Project, 2022) and except for a handful of independently run spectrometer networks, data provided by the NOVAC network offers the only continuous daytime recording of volcanic SO_2 emissions (Galle et al., 2010). The NOVAC Database (NOVAC Project, 2020) contains time series of SO_2 emissions for 32 of these volcanoes, between 2005 and 2017, but the completeness of the data is variable (Figure 1). Emissions of SO_2 are derived from radiance spectra which are recorded by a series of instruments which scan the horizon at steps of 3.6°. Each of these spectra are analyzed using DOAS technique to retrieve a Slant Column Density (SCD) of SO_2 from spectra with elevation angles ranging from ±90° from zenith. Resulting SCDs are used to estimate the plume's angular center-of-mass and thereby its location before converting SCDs to Vertical Column Densities

21699356, 2022, 12, Downloaded from https://agupubs.onlinelibrary.wiley.com/doi/10.1029/2022JB025380 by Cochrane France, Wiley Online Library on [05/01/2023]. See the Terms and Conditions (https://onlinelibrary.wiley.com/terms-and-conditions) on Wiley Online Library for rules of use; OA articles are governed by the applicable Creative Commons License

Table 1
Description of Parameters Included in the NOVAC Database (Arellano et al., 2021)

Parameter	Description	Units	Details
SO_2 emission rate	Daily mean of observed SO_2 emission rate	kg s^{-1}	Calculated when >5 valid measurements are available for the day.
Plume speed	Daily mean of used plume speed	m s^{-1}	Wind velocity obtained from the ERA-Interim database (Dee et al., 2011) of ECMWF is used, with a grid resolution of 0.125 × 0.125°, 6 hr and up to 60 vertical levels from ground up to 0.1 hPa. Data are interpolated to the location of the volcanic vent and time of measurement for each emission rate calculation. Atmospheric pressure is converted to vertical height using the L60 model definitions of ECMWF (U.S. Standard Atmosphere, 1976).
Plume direction	Daily mean of observed plume direction	Degrees (°)	The volcanic plume is located using its angular center-of-mass determined by the measured SCDs. Its direction may be estimated from triangulation of two scans (Johansson et al., 2009).
Plume altitude	Daily mean of observed plume altitude	m asl	Plume altitude can be estimated from triangulation of two scans (Johansson et al., 2009) or is assumed to be the summit altitude.
Distance to plume	Daily mean of observed distance to plume	M	Retrieved from measurement.
Plume width	Daily mean of plume width scanned by instrument(s)	M	Retrieved from measurement.
Cloud cover	Daily mean of modeled cloud cover at summit altitude	%	Cloud cover is taken from the ERA-Interim database (Dee et al., 2011) of ECMWF, retrieved every 6 hr on a horizontal grid of 0.125 × 0.125° (13.9 × 13.9 km for mean Earth radius) surrounding the location of the main volcanic vent. It is then further interpolated to the vent location and the time of each scan.
Total measurements	Number of total scan measurements on each day	n.a.	All measurements of SO_2 emission rate on each day.
Valid measurements	Number of valid SO_2 emission rate measurements on each day	n.a.	A single measurement of SO_2 emission is considered valid if it has a minimum number of valid SCDs in the scan and almost complete coverage of the plume (completeness factor >0.8).

(VCDs) using a geometrical approximation of the air-mass factor (AMF). The baseline SCD is estimated from the lowest 20% of valid SCDs and subtracted from all spectra (Galle et al., 2010). The total SO_2 in a cross section of the plume is then calculated by treating each set of two neighboring slant column measurements as a single section, where the average VCD between the two measurements is multiplied by the width of that segment to give the total SO_2 within a section of the plume. Taking the sum of all segments, an Integrated Column Amount (ICA) is obtained. Multiplying this ICA by the normal component of the plume velocity gives an SO_2 emission rate that is commonly reported in kg s^{-1} (Arellano et al., 2021). Emission rates of SO_2 incorporated in the NOVAC Database are calculated using wind speed from a reanalysis data set (Dee et al., 2011) provided by the European Centre for Medium-Range Weather Forecasts (ECMWF) to represent plume speed (Arellano et al., 2021). Table 1 gives a brief description of the parameters, in addition to the measured SCD, which contribute to generating the reported daily SO_2 emission rate. Some parameters are obtained from the (modeled) meteorological data set (e.g., cloud cover), some are measured (e.g., plume width) and some refer to the validity of measurements (e.g., number of total and valid measurements in a day). Each parameter may therefore have a different contribution to the final

21699356, 2022, 12, Downloaded from https://agupubs.onlinelibrary.wiley.com/doi/10.1029/2022JB025380 by Cochrane France, Wiley Online Library on [05/01/2023]. See the Terms and Conditions (https://onlinelibrary.wiley.com/terms-and-conditions) on Wiley Online Library for rules of use; OA articles are governed by the applicable Creative Commons License

reported SO_2 emission rate and associated uncertainty. When more than five valid measurements are available for a single day, the daily average (arithmetic mean) and standard deviation of the reported variables are recorded, and it is this time series which is made available via the NOVAC Database (NOVAC Project, 2020) and which we have used in this study (Figure A1).

2.2. Error in the Time Series of SO_2 Emission Rate

Error in the reported SO_2 emission rate arises from uncertainty in the measurement of SO_2 (e.g., spectroscopic error), as well as the variables used to derive emission rates (e.g., wind speed). The SO_2 emission rates used in this study, despite noncontinuous, are considered to have good quality. Compared to typical NOVAC measurements where total error may exceed 100% in poor conditions (Galle et al., 2010), SO_2 emissions data in the NOVAC Database, which are used in this study, have a minimum uncertainty estimate between −30% and 10%. One of the biggest challenges in deriving accurate SO_2 emission rates is obtaining accurate wind speeds at the altitude of the volcanic plume (Arellano et al., 2021). In addition to plume velocity, the main source of uncertainty is atmospheric and in-plume scattering which contribute to error in the spectroscopic retrieval of SO_2 (Kern et al., 2010; Millan, 1980). Since the error associated with each individual measurement of SO_2 emission is not provided, we incorporate the standard deviation of the daily SO_2 emission rates in our analysis.

2.3. Calculating Power Spectral Density Estimates

A challenge when applying common time series analysis techniques is the occurrence of datagaps. Datagaps are common in ground-based remote sensing data, and correspond to periods of little volcanic degassing, when no SO_2 is detected, but also when there is a large deviation in prevailing wind conditions, so that the plume is not visible by the instrument network (Arellano et al., 2021; Galle et al., 2010). Combined with instrument failure (during power outage e.g.), time series of volcanic SO_2 emission rates typically contain large and frequent datagaps. Here, we use the Lomb-Scargle periodogram (Lomb, 1976; Scargle, 1982), a technique which has been adopted by the volcano-gas community (e.g., Dinger et al., 2018; Pering et al., 2019; Sweeney et al., 2008) which allows efficient computation of a Fourier-like power spectrum from unevenly sampled data. Using the Lomb-Scargle approach, we can overcome the challenge of excessive datagaps to analyze time series of SO_2 emissions for periodic trends.

The Lomb-Scargle method weights the time series on a per-point basis, rather than in time, and thus provides a means of frequency analysis without incorporating data-filling techniques that would be required for regularizing time series of volcanic SO_2 emissions. The Lomb-Scargle periodogram provides a Fourier-like power spectrum estimate, the so-called Power Spectral Density (PSD) which is a measure of the signal's power content as a function of frequency and reveals the period of oscillations contained in the time series (VanderPlas, 2018). As is the case for frequency analysis techniques, the Lomb-Scargle method can be used to detect periodicities at frequencies between twice the sampling rate and half the data set length (Nyquist, 1928). We considered the daily mean SO_2 emission rate and also incorporate the standard deviation to account for the large variation in SO_2 emission rates recorded throughout the day. We applied a bootstrapping approach to calculate the PSD from resampled time series of the daily SO_2 emission rates 1,000 times, each time selecting a random value (mean ± standard deviation). By doing so we assume the distribution of values is uniform for each day which is not always the case. While the first, second, and third quartiles of daily SO_2 emission rates are included in the NOVAC Database, we have taken this standard approach to enable the comparison of PSD between parameters (Table 1) where percentile information is not provided.

We used MATLAB's Plomb function (MathWorks, 2021) to calculate the Lomb-Scargle periodogram of each bootstrapped time series. Since the SO_2 emission rate is reported as a daily mean, we use a sampling rate (ΔT) of 1 day to calculate the PSD estimate. We use an oversampling factor (*ofac*) of four, which resembles the zero-padding technique for FFT-based methods and is used to improve the resolution of the frequency grid over which the PSD is calculated. The maximum frequency is determined by $1/(2 \times \Delta T)$, which for uniformly spaced signals corresponds to the Nyquist frequency (Nyquist, 1928). We refer to this here as the pseudo-Nyquist frequency, which represents the shortest period we are capable of detecting based on the ΔT (2 days). The minimum frequency is defined by $1/(ofac \times N \times \Delta T)$, where N is the number of days between the start and end dates of the time series and not necessarily the number of datapoints. We further limit the frequency when reporting

21699356, 2022, 12, Downloaded from https://agupubs.onlinelibrary.wiley.com/doi/10.1029/2022JB025380 by Cochrane France, Wiley Online Library on [05/01/2023]. See the Terms and Conditions (https://onlinelibrary.wiley.com/terms-and-conditions) on Wiley Online Library for rules of use; OA articles are governed by the applicable Creative Commons License

the PSD estimates, to consider periods between the pseudo-Nyquist frequency and $N/4$, corresponding to 2 days and four-cycles per time series, e.g., 497 days at Mayon since the time series is 1991 days in length. We therefore exclude periodicities with only two or three complete cycles. Four volcanoes did not have enough datapoints to calculate PSD while adhering to the above criteria ($N \leq 8$), and so we do not report results for Sangay (Ecuador), San Miguel (El Salvador), and Llaima and Planchón-Peteroa (Chile).

We performed the same analysis for all parameters included in Table 1 for the purpose of determining the source of any periodicities in the SO_2 emission rate. Since for each volcano all parameters have the same sampling, comparing the PSD estimates across parameters also serves to highlight potential artifacts. Since the total number of measurements and number of valid measurements do not have associated standard deviations, these parameters were not bootstrapped.

2.4. False-Alarm Probabilities

To determine if any peaks in the PSD estimate are significant and therefore indicate a periodicity in the time series, we used False-Alarm Probabilities (FAPs). These provide the probability of measuring a peak of a given height (or higher) if the data were to consist of Gaussian noise with no periodic component. To characterize whether the time series we have analyzed contains periodicities, we calculated FAPs of 50%, 10%, 1%, and 0.01%, using the Plomb function (MathWorks, 2021). For example, considering a 10% FAP and several data samples with no periodic signal, a peak in the PSD estimate of a given height or above will occur in just 10% of the samples. If the returned PSD estimate of our time series data produces a peak of that height, the null hypothesis, that no periodic trend is present in the time series, can be rejected with 90% confidence. Crucially, FAPs do not give a probability that the time series is periodic but rather provides a confidence level in rejecting the null hypothesis. We consider a periodicity to be statistically significant, if the median PSD reaches at least the 50% FAP threshold, enabling us to reject the null hypothesis, in favor of a true periodic signal, with a confidence level of 50% or more. Since only one PSD estimate is determined for the total number of measurements and number of valid measurements, we consider a periodicity in these parameters to be statistically significant if the returned PSD reaches the 50% FAP threshold. We use this conservative threshold to account for the possible reduction in PSD estimates of real periodic trends when multiple periodicities exist in the time series (Appendix B).

2.5. Synthetic Signal

We tested the use of the Lomb-Scargle approach by applying it to two synthetic signals of known periodicities. We produced a synthetic signal with a periodicity of 50 days, and a second one with two additional periodicities of 14 and 180 days. We chose 14 days since its close to the period of the lunisolar fortnightly (M_f) tidal component (~13.7 days), and 180 days since its close to the maximum frequency considered for several volcanoes (Section 2.3). Gaussian noise was added to the synthetic signals which represented the signal-to-noise ratio (*snr*) of time series data, defined as the mean of the daily standard deviation divided by the daily mean SO_2 emission rate. The noisy synthetic signal was then rescaled within the respective ranges of daily mean SO_2 emission and resampled to match the days for which an SO_2 emission rate is available at Mayon, Philippines (Appendix B) and Concepción, Nicaragua (Figure 2). These two volcanoes were used because their time series of SO_2 emissions have significant datagaps and therefore provide a cautious assessment of our approach. Figure 2 demonstrates the capability of the Lomb-Scargle periodogram to identify multiple periodicities in the time series of SO_2 emission despite large datagaps. The median PSD estimates cross the 10% FAP threshold at 14 and 180 days (Figure 2). PSD estimates for the two periodicities are comparable, reflecting their equal contribution to the synthetic signal. Although symmetrical peaks surround the identified periodicities, they fail to reach the 50% FAP threshold. The median PSD estimate associated with the 50-day periodicity also fails to reach the 50% FAP threshold, highlighting the possibility of missing genuine periodic trends when multiple periodicities exist. Crucially, however, the peak at 50 days remains pronounced and is clearly distinguishable from background PSD estimates. Figure 2 highlights one limitation of using FAPs. Several median PSD estimates close to the 180-day periodicity cross the 50% FAP threshold, yet it is the highest PSD estimate which corresponds to the true 180-day periodicity (with FAP 10%) (Figure 2).

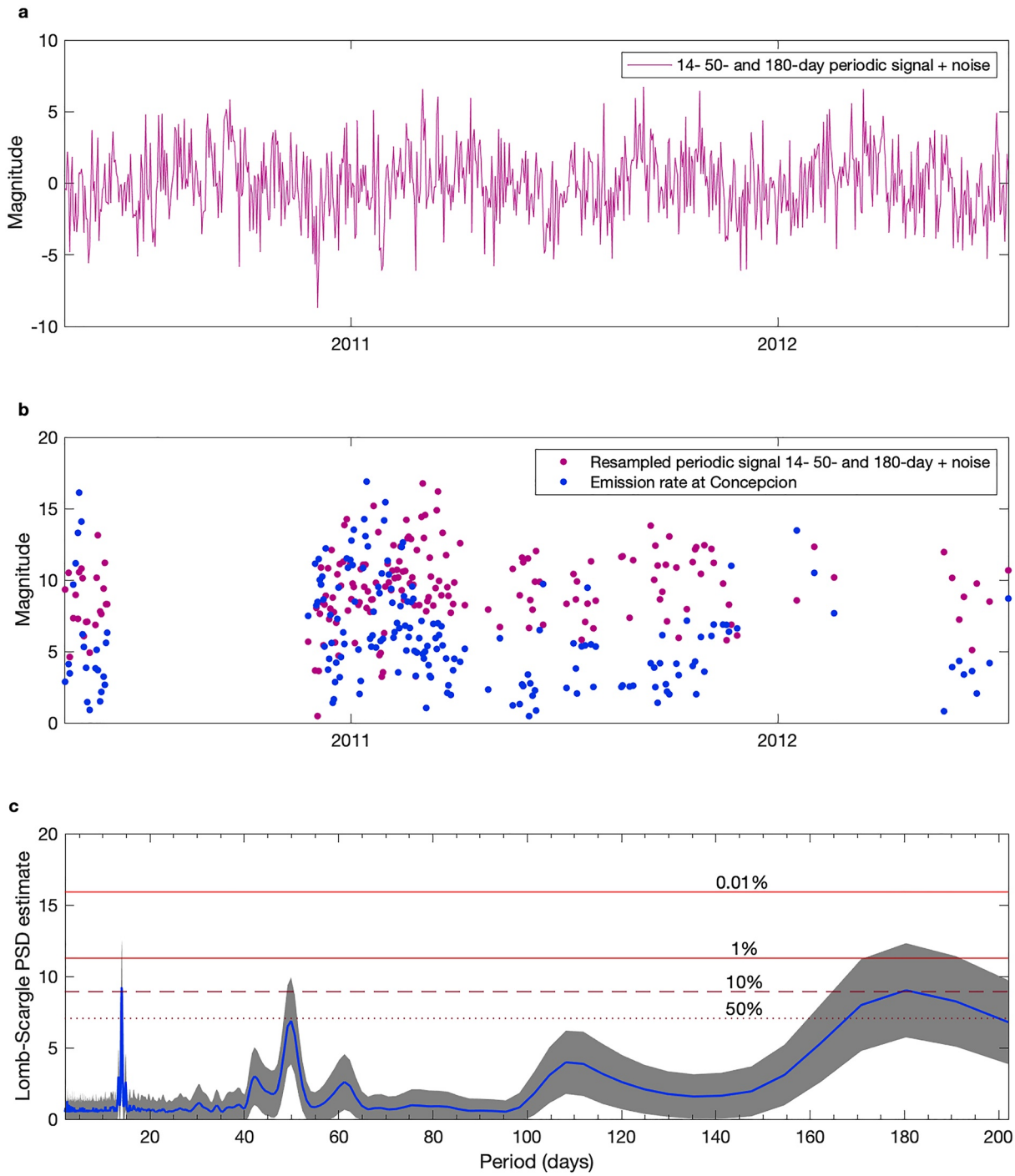

Figure 2. (a) Synthetic signal with periodicities of 14, 50, and 180 days with Gaussian noise added to the synthetic signal using MATLAB function "aywgn" (MathWorks, 2021). We used "measurement" and "linear" as function inputs to measure the power of the synthetic signal and apply Gaussian noise equivalent to the *snr* at Concepción. We define the *snr* as the mean of daily standard deviation divided by the daily SO_2 emission rate (0.33). (b) The noisy synthetic signal is rescaled and resampled to match the magnitude of SO_2 emission rates and the days for which an SO_2 emission rates are available at Concepción. (c) Median (blue line) and standard deviation (gray shaded) of Lomb-Scargle Power Spectral Density (PSD) estimates from 1,000 signals, all with periodicities of 14, 50, and 180 days but with different Gaussian noise applied. All signals were scaled and resampled to match the magnitude of SO_2 emission rates reported and the days for which an SO_2 emission rate is available at Concepción volcano.

21699356, 2022, 12, Downloaded from https://agupubs.onlinelibrary.wiley.com/doi/10.1029/2022JB025380 by Cochrane France, Wiley Online Library on [05/01/2023]. See the Terms and Conditions (https://onlinelibrary.wiley.com/terms-and-conditions) on Wiley Online Library for rules of use; OA articles are governed by the applicable Creative Commons License

21699356, 2022, 12, Downloaded from https://agupubs.onlinelibrary.wiley.com/doi/10.1029/2022JB025380 by Cochrane France, Wiley Online Library on [05/01/2023]. See the Terms and Conditions (https://onlinelibrary.wiley.com/terms-and-conditions) on Wiley Online Library for rules of use; OA articles are governed by the applicable Creative Commons License

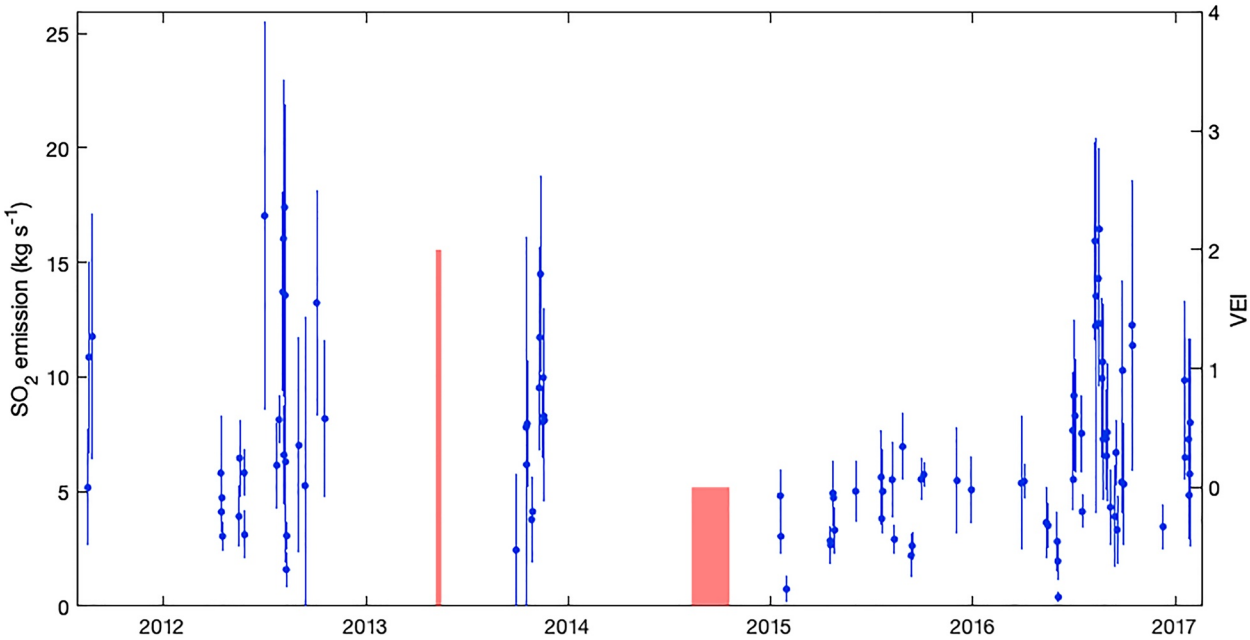

Figure 3. Emission rate of SO_2 at Mayon volcano, Philippines. Daily mean SO_2 emission rates are plotted as blue circles and error bars represent the corresponding standard deviation (Bornas et al., 2020). Eruptive activity is represented by red bars, using confirmed eruptions as defined in the Smithsonian's Global Volcanism Program database (Global Volcanism Program, 2013b).

3. Results and Discussion

3.1. Mayon Volcano

The time series of daily mean SO_2 emissions at Mayon volcano, Philippines (Bornas et al., 2020) vary between about <1 and 17 kg s^{-1}, as described by 102 data points between August 2011 and January 2017, corresponding to about 5% of days with data (Figure 3). The variation of SO_2 emission rates obtained from measurements within any single day may exceed 17 kg s^{-1}. The Lomb-Scargle PSD median estimates for the time series of SO_2 emission rate between August 2011 and January 2017 are below the 50% FAP threshold, except for one peak at 51 days and another at 99 days which surpass the 1% and 50% FAP thresholds, respectively (Figure 4). We also performed Lomb-Scargle analysis on the range of parameters involved in the calculation of the SO_2 emission rate and found that only the plume speed obtained from the ECMWF ERA-Interim database (see Table 1) has corresponding 51-day and 99-day periodicities with FAPs of 1% (51 days) and 50% (99 days) (Figure 5).

We find that other common periodicities are commonly present in the parameters involved in the calculation of the SO_2 emission rate at Mayon (Table 2). At longer periods, PSD estimates of plume direction and distance to plume indicate periodicities at 187 and 298 days, the 187-day periodicity also found in the PSD estimate of total measurements. Since the instrument network is fixed, the same plume direction implies a similar distance (assuming similar plume altitude) from the measuring instrument, and therefore if a periodic trend exists in plume direction, it may also be expected in the distance to plume. These periodicities of roughly 6 and 10 months are likely associated with the two main seasons which determine the prevailing wind across southern Luzon, Philippines. Neither of these longer periods are associated with statistically significant periodicities in the emission of SO_2 at Mayon. This finding suggests that the reported SO_2 emissions are not influenced in a systematic manner by the seasonal shift in plume position. There is no statistically significant periodicity in the SO_2 emission rate at ~14 days, nor a spike in PSD estimate, which could correspond to the M_f tidal constituent (Figure 4).

Our analysis shows common periodicities in the emission rate of SO_2 and plume speed, but these are not identified in the other parameters. We can therefore rule out the possibility that the identified periodicities are artifacts due to the datagaps in the time series. Detailed analysis shows that the PSD estimates of plume speed and SO_2 emission rates are positively correlated (Figure 6). Analysis of the relationships between the PSD of the SO_2 and of the plume speed allows us to identify four main fields according to the values of the FAPs, and which are

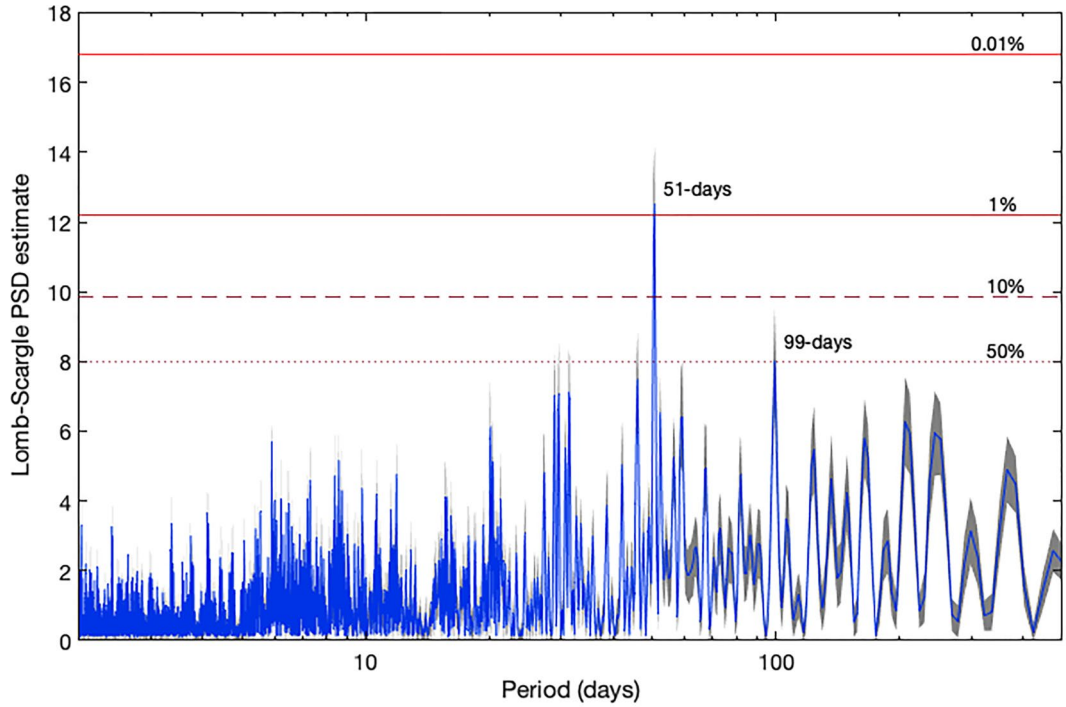

Figure 4. Lomb-Scargle Power Spectral Density (PSD) estimate of SO_2 emission rate at Mayon volcano between the pseudo-Nyquist frequency and $N/4$, corresponding to 2 days and four-cycles per time series ($N/4 = 497$ days at Mayon). Blue line corresponds to the median PSD estimate obtained by resampling the time series of SO_2 emission rate 1,000 times, between the minimum and maximum values on any given day. Standard deviation of the returned PSD estimates is shown in gray. Horizontal lines represent the corresponding False-Alarm Probability (FAP) threshold values. Periodicities are considered statistically significant if the median PSD reaches the 50% FAP threshold, enabling rejection of the null hypothesis with at least 50% confidence. Statistically significant periodicities are labeled.

useful to clarify the significance of the two variables in a systematic manner (Figure 5). Most data plots below the 50% FAP for both parameters. The PSD estimates which are statistically significant (FAP of 50% or less), either reach the same FAP threshold in both plume speed and SO_2 emission rate, or PSD estimates of plume speed are associated with lower FAPs than those of SO_2 emission rate. An apparent correlation between PSD estimates in SO_2 emission rate and those in-plume speed make a strong case for the source of observed periodicities at Mayon originating from wind speed used to calculate SO_2 emissions (Figure 5).

Availability of SO_2 emission rates at Mayon are concentrated during northern-hemisphere summer months (Figure 2). During this time westerly winds blowing to the east gradually dominate over the prevailing trade winds, resulting in a gradual increase in wind speeds which run parallel to the Equator. Over southeast Luzon, these zonal winds reach maximum speeds in mid-July before gradually subsiding until the start of the next monsoon in October, when easterly trade winds dominate (Matsumoto et al., 2020). To determine if periodicities exist in the zonal wind speed at Mayon volcano, we performed the Lomb-Scargle analysis using a complete ECMWF time series of the absolute zonal wind speed (Figure 7). A 51-day periodicity is identified with an FAP of 0.01% which is likely associated with the well-known 30–60-day Madden-Julian Oscillation (MJO) responsible for intraseasonal variability in the tropical atmosphere (Madden & Julian, 1971, 1972, 1994).

While ocean loading around Mayon due to Earth tides has been identified as a possible trigger for eruptions at Mayon (Jentzsch et al., 2001), our analysis does not identify a fortnightly periodicity in the emission rate of SO_2. Previous studies at Mayon have found high frequency cycles in H_2O emissions with several periodic components in the order of minutes (Girona et al., 2015). These are shorter than the minimum periodicities detectable in the time series data used in this study and thus, we are unable to compare periodic trends in SO_2 emission rates with those found for other plume gases.

21699356, 2022, 12, Downloaded from https://agupubs.onlinelibrary.wiley.com/doi/10.1029/2022JB025380 by Cochrane France, Wiley Online Library on [05/01/2023]. See the Terms and Conditions (https://onlinelibrary.wiley.com/terms-and-conditions) on Wiley Online Library for rules of use; OA articles are governed by the applicable Creative Commons License

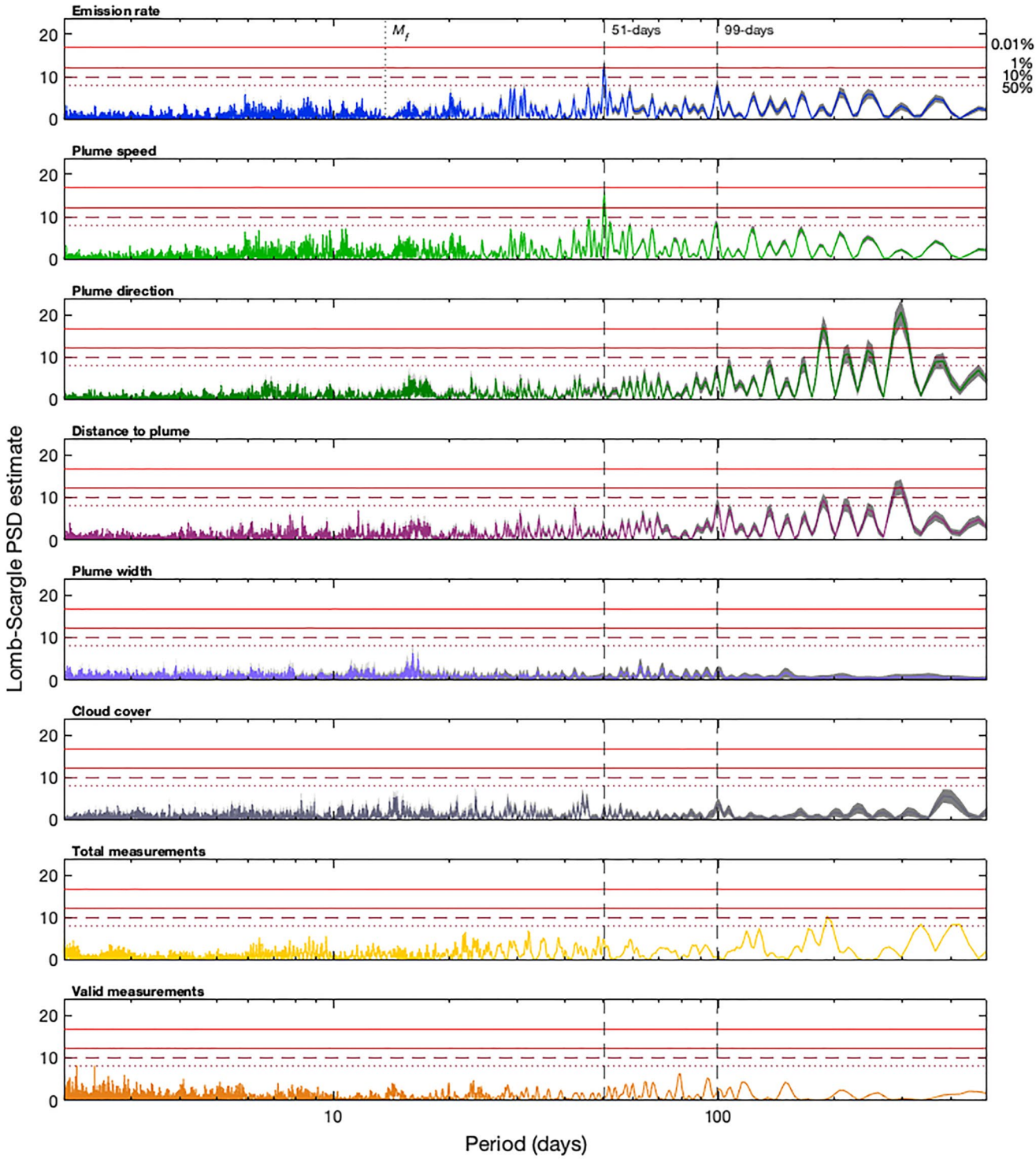

Figure 5.

3.1.1. Other Volcanoes in the NOVAC Database

We applied the same methodology to 28 volcanoes of the NOVAC network and we found multiple median PSD estimates which reach the 50% FAP threshold (Figure C1). Several periodicities have FAPs of 0.01%, enabling the rejection of the null hypothesis (that no periodic trend exists) with at least 99.99% confidence. We found that

21699356, 2022, 12, Downloaded from https://agupubs.onlinelibrary.wiley.com/doi/10.1029/2022JB025380 by Cochrane France, Wiley Online Library on [05/01/2023]. See the Terms and Conditions (https://onlinelibrary.wiley.com/terms-and-conditions) on Wiley Online Library for rules of use; OA articles are governed by the applicable Creative Commons License

21699356, 2022, 12, Downloaded from https://agupubs.onlinelibrary.wiley.com/doi/10.1029/2022JB025380 by Cochrane France, Wiley Online Library on [05/01/2023]. See the Terms and Conditions (https://onlinelibrary.wiley.com/terms-and-conditions) on Wiley Online Library for rules of use; OA articles are governed by the applicable Creative Commons License

Table 2
Periodicities in the Time Series of SO_2 Emission Rate at Mayon Volcano, Which Are Also Identified in the Time Series of Associated Parameters, and Their Corresponding FAP Thresholds

Periodicity (days)	Parameters	FAP threshold (%)
51	**SO_2 emission rate**	**1**
	Plume speed	**1**
99	**SO_2 emission rate**	**50**
	Plume speed	**50**
187	Plume direction	0.01
	Distance to plume	50
	Total measurements	1
298	Plume direction	0.01
	Distance to plume	1

Note. Where adjacent peaks in PSD estimates reach the 50% FAP threshold, we consider the highest PSD estimate only. Rows where the periodicity is identified in the SO_2 emission rate at Mayon are in bold. No periodicities were identified in the time series of plume width or cloud cover.

many volcanoes show a similar trend to the Mayon data, whereby periodicities identified in the time series of SO_2 emission rates are also present in the plume speed used to derive these emission rates (Figure 8).

We attempted to summarize these relationships by categorizing volcanoes in four different fields according to the periodicities found in SO_2 emission rate and plume speed (Figures 6 and 9). Periodicities were not identified (FAP > 50%) in either parameter at six of the volcanoes (21% of the total): Arenal, Copahue, Fuego, Piton de la Fournaise, Santa Ana, and Vulcano. Except for Copahue, these volcanoes have time series of SO_2 emission rate with very few data (Piton de la Fournaise and Vulcano) or particularly sparsely populated time series (Arenal, Fuego, and Santa Ana; Figure A1). Emission rates of SO_2 are available for a 2-year timespan at Copahue. While most data are missing for the latter half of 2016, a more or less continuous time series exists from the end of 2014 to 2016. The lack of prominent peaks in the PSD estimates suggests no significant periodic trends in the order of day to weeks exist in the SO_2 emission rate from Copahue during 2015.

Where periodicities in the SO_2 emission rate were identified, we found 14 volcanoes (50%) which had corresponding periodicities in the PSD estimates of plume speed (Figure 9). Twenty volcanoes (71% of the total) revealed periodicities in the plume speed used to determine SO_2 emission rates but not in the emission rate of SO_2. Ten volcanoes (36%) were found to have at least one periodicity in the SO_2 emission rate, which was unaccompanied by the same periodicity in-plume speed. To understand the nature of the periodicities in the SO_2 emission rate at these 10 volcanoes, we did a visual inspection of the Lomb-Scargle periodogram for all parameters. Periodicities of 50, 57, and 70 days in the SO_2 emission rate at Etna volcano correspond to prominent peaks in the PSD estimate of plume speed, despite that the latter do not quite reach the 50% FAP threshold (Figure 10). Our analysis of synthetic signals highlights the possibility of missing genuine periodic trends when multiple periodicities are present (Figure 3). A significant 39-day periodicity in the plume speed at Etna may have the effect to reduce the magnitude of the 50-day, 57-day, and 70-day PSD estimates. Since these peaks remain pronounced and the Lomb-Scargle periodogram for the two parameters appear similar, the identified periodicities in SO_2 emission rate at Etna are likely associated with periodicities in-plume speed. Several longer periodicities identified in the SO_2 emission rate were slightly offset from periodicities in-plume speed (e.g., 180 days at Masaya) or were accompanied by periodicities in other parameters (Appendix D). Two periodicities identified in the SO_2 emission rate at Fuego de Colima (both associated with FAPs of 50%) appear not to be associated with periodicities in any other parameter we analyzed and therefore may be of volcanic origin (Figure 11).

3.2. Wind Speeds and Volcanic Degassing

We have identified periodicities in SO_2 emission rate which are associated with common periodicities in the plume speed used to derive them. For the case of Mayon and Masaya (both in the tropics), we confirm that periodicities in the plume speed arise due to periodic behavior of the trade winds by analyzing complete time series of zonal wind speeds (Figure 12). These findings imply a systematic relationship between reported SO_2 emission rates and wind speed which suggest (a) a causal relationship whereby wind speed influences the volcanic system

Figure 5. Lomb-Scargle Power Spectral Density (PSD) estimate of SO_2 emission rate at Mayon together with PSD of parameters used to determine SO_2 emission rate between the pseudo-Nyquist frequency and $N/4$, corresponding to 2 days and four-cycles per time series ($N/4 = 497$ days at Mayon). Median PSD estimates for each parameter are shown as single solid line obtained by resampling the time series 1,000 times, between the minimum and maximum values on any given day. Standard deviation of the returned PSD estimates is shown in gray. Total measurements and valid measurements are the exception for which the PSD estimate was calculated only once. Horizontal lines represent the threshold values corresponding to False-Alarm Probabilities (FAPs) of 50% (8.0), 10% (9.9), 1% (12.2), and 0.01% (16.8). Periodicities are considered statistically significant if the median PSD reaches the 50% FAP threshold, enabling rejection of the null hypothesis with at least 50% confidence. Since only one PSD estimate is determined for the total number of measurements and number of valid measurements, we consider a periodicity in these parameters to be statistically significant if the returned PSD reaches the 50% FAP threshold. Statistically significant periodicities in the time series of SO_2 emission rate are labeled. A dotted vertical line indicates the period of the M_f tidal constituent (~13.7 days), which is the fortnightly tide associated to lunar cycles. Note that for the case of Mayon volcano, there is no variation in the observed plume altitude parameter and therefore the Lomb-Scargle PSD estimate was not calculated for this parameter.

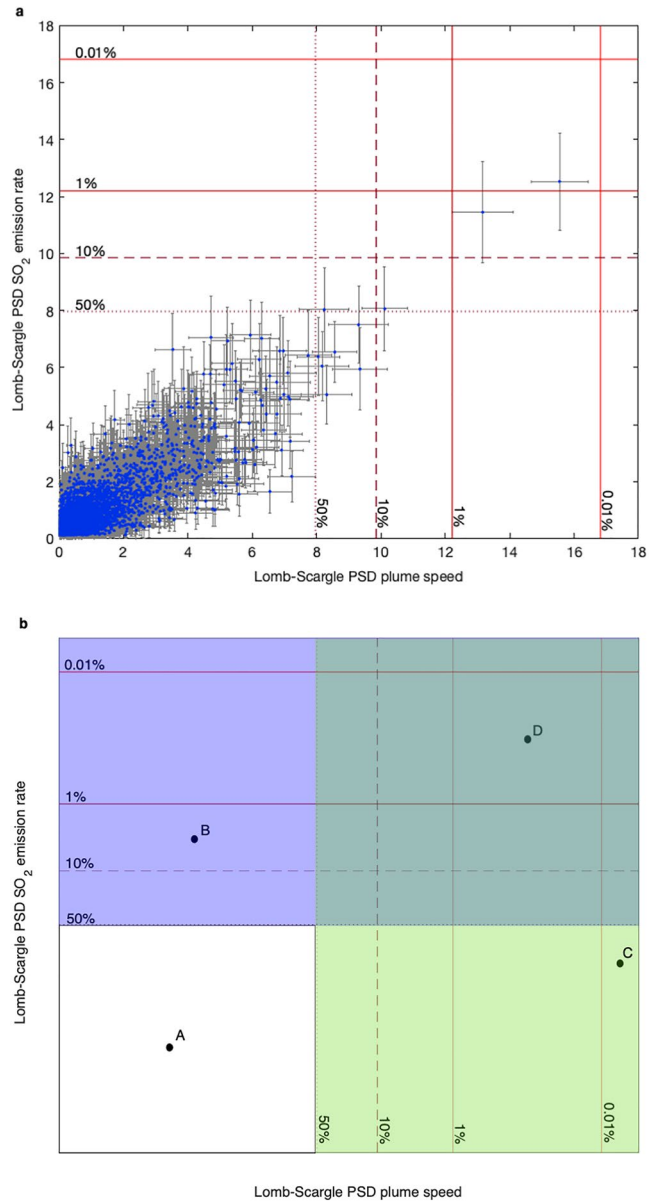

Figure 6. Relationships and significance of Power Spectral Density (PSD) of SO_2 emission rates and plume speeds for Mayon volcano between August 2011 and January 2017. (a) Lomb-Scargle PSD estimate of plume speed used to calculate SO_2 emission rate and PSD estimate of SO_2 emission rate between the pseudo-Nyquist frequency and *N*/4, corresponding to 2 days and four-cycles per time series. Datapoints are the median PSD estimate and error bars are the standard deviation. Horizontal and vertical lines represent the threshold values corresponding to False-Alarm Probabilities (FAPs) of 50% (8.0), 10% (9.9), 1% (12.2), and 0.01% (16.8) for SO_2 emission rate and plume speed, respectively. (b) Schematic classification of the relationships and significance of the PSD of SO_2 emission rates and plume speeds according to FAP values. Marker A (in white area) corresponds to datapoints clustered below the 50% FAP in panel (a) and are most PSD estimates that are not statistically significant in the time series of SO_2 emission rate and plume speed. The blue area are periodicities in SO_2 emission rate without accompanying periodicities in the plume speed. The bright green area are periodicities in-plume speed that are unaccompanied by periodicity in SO_2 emission rate. The dark green area are periodicities present in both the SO_2 emission rate and plume speed. FAPs provide a further constraint on the significance of the identified periodicity. For example, if a datapoint occupies the position of marker B, PSD estimates in SO_2 emission rate surpasses the 10% FAP threshold, enabling the rejection of the null hypothesis with at least 90%. Marker C indicates a datapoint whereby a PSD estimates in-plume speed enable the rejection of the null hypothesis with at least 99.99%. At marker D, a datapoint would indicate both periodicities to be associated with an FAP of 1%, enabling rejection of the null hypothesis with at least 99% confidence.

21699356, 2022, 12, Downloaded from https://agupubs.onlinelibrary.wiley.com/doi/10.1029/2022JB025380 by Cochrane France, Wiley Online Library on [05/01/2023]. See the Terms and Conditions (https://onlinelibrary.wiley.com/terms-and-conditions) on Wiley Online Library for rules of use; OA articles are governed by the applicable Creative Commons License

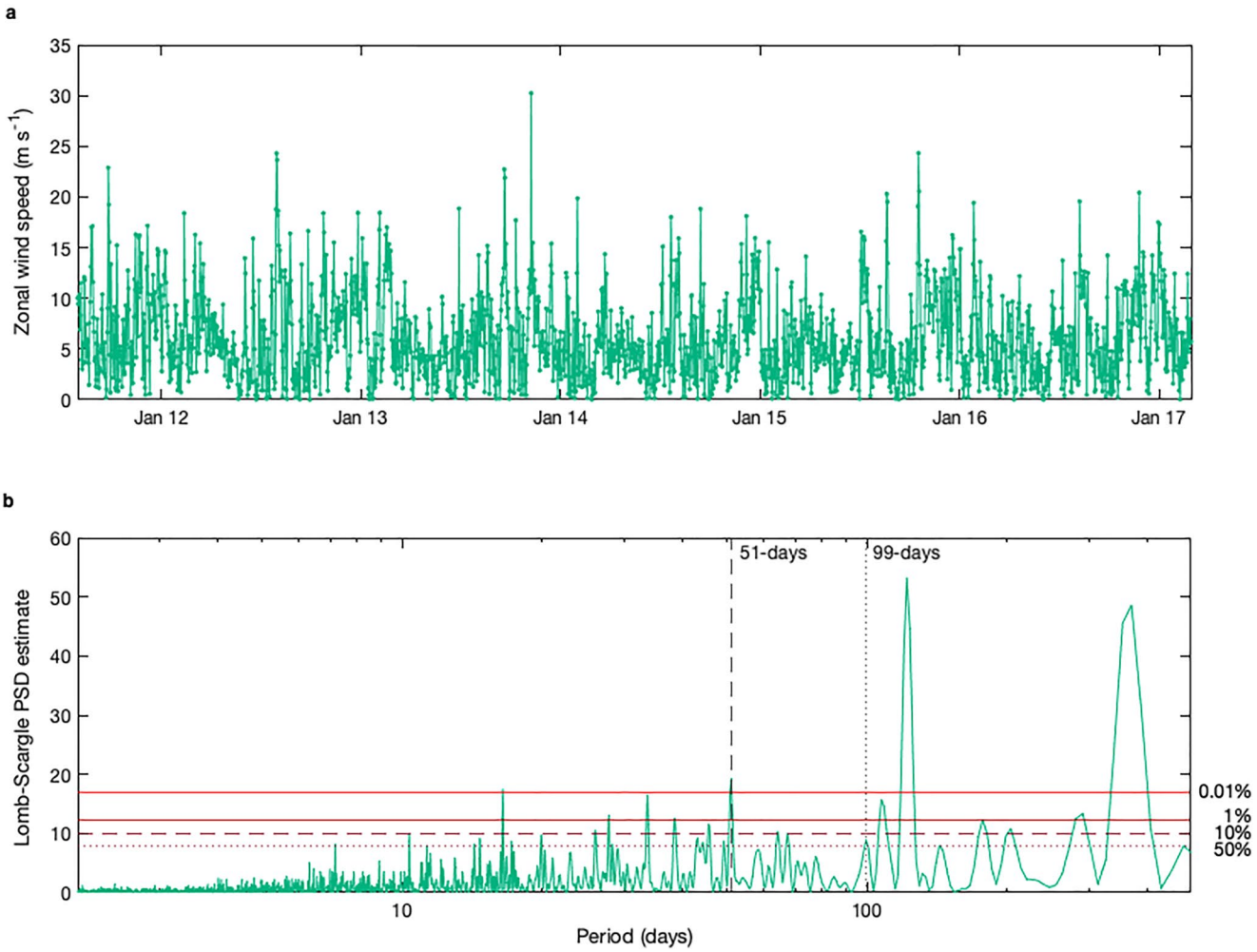

Figure 7. (a) Continuous time series of the magnitude of zonal wind speed at Mayon volcano. Atmospheric specifications are provided by the European Centre for Medium-Range Weather Forecasts (ECMWF, 2022) operational High spatial RESolution forecasts (HRES) products with 137 levels (cycle 38r2). Wind speed information is extracted for the latitude and longitude closest to Mayon volcano (13.5°N and 123.5°E) and at atmospheric level closest to the plume altitude used for determining SO_2 emission rate (2,370 m asl). (b) Lomb-Scargle Power Spectral Density (PSD) estimate of zonal wind speeds. Horizontal lines correspond to False Alarm Probability (FAP): 50% (8.0), 10% (9.9), 1% (12.2), and 0.01% (16.8). A vertical dashed line indicates the 51-day periodicity identified in the SO_2 emission rate (Figure 2) and it is also identified in the zonal wind component at Mayon volcano. Associated with an FAP of 0.01% FAP, we may reject the null hypothesis with >99.99% confidence. A dotted vertical line corresponds to the 99-day periodicity identified in the SO_2 emission rate (Figure 2). The PSD estimate of the zonal wind component at 99 days reaches the 50% FAP threshold. Since the PSD estimate is calculated for a single data set, we may cautiously reject the null hypothesis as ~50% of signals without a periodic trend would result in a PSD peak of the same magnitude. Periodicities at 16, 122, and 371 days are also identified with an FAP 0.01%, together with several additional peaks in PSD with FAP < 50%, indicating zonal wind speed at Mayon is highly periodic.

and thereby the emission of SO_2, (b) a common causation for periodicity in both wind speed and the volcanic degassing of SO_2, (c) wind speeds affect downwind measurements of SO_2 emission rate, or (d) systematic bias in deriving SO_2 emission rates using wind speeds. Since influence (if any) from volcanic degassing is not incorporated in the ECMWF ERA-Interim data (Dee et al., 2011), we can exclude the possibility that plume gases modulate model wind speeds. We discuss the plausibility of cases (a) to (c) below.

3.2.1. Influence of Wind Speed on the Volcanic System and Its Emissions of SO_2

Surface loads generated from strong winds can trigger rockfalls and landslides which could be proposed to contribute to increased SO_2 emissions (Bredemeyer & Hansteen, 2014). This effect is likely limited to episodes of dome growth at passively degassing volcanoes. However, most volcanoes considered in this study, during the period for which SO_2 emissions were analyzed, had at least one explosive eruption and several did not exhibit lava dome growth (e.g., Cotopaxi, Turrialba; Global Volcanism Program, 2013a). We therefore consider it improbable strong winds explain the systematic influence on the emission rate of SO_2.

21699356, 2022, 12, Downloaded from https://agupubs.onlinelibrary.wiley.com/doi/10.1029/2022JB025380 by Cochrane France, Wiley Online Library on [05/01/2023]. See the Terms and Conditions (https://onlinelibrary.wiley.com/terms-and-conditions) on Wiley Online Library for rules of use; OA articles are governed by the applicable Creative Commons License

10.1029/2022JB025380

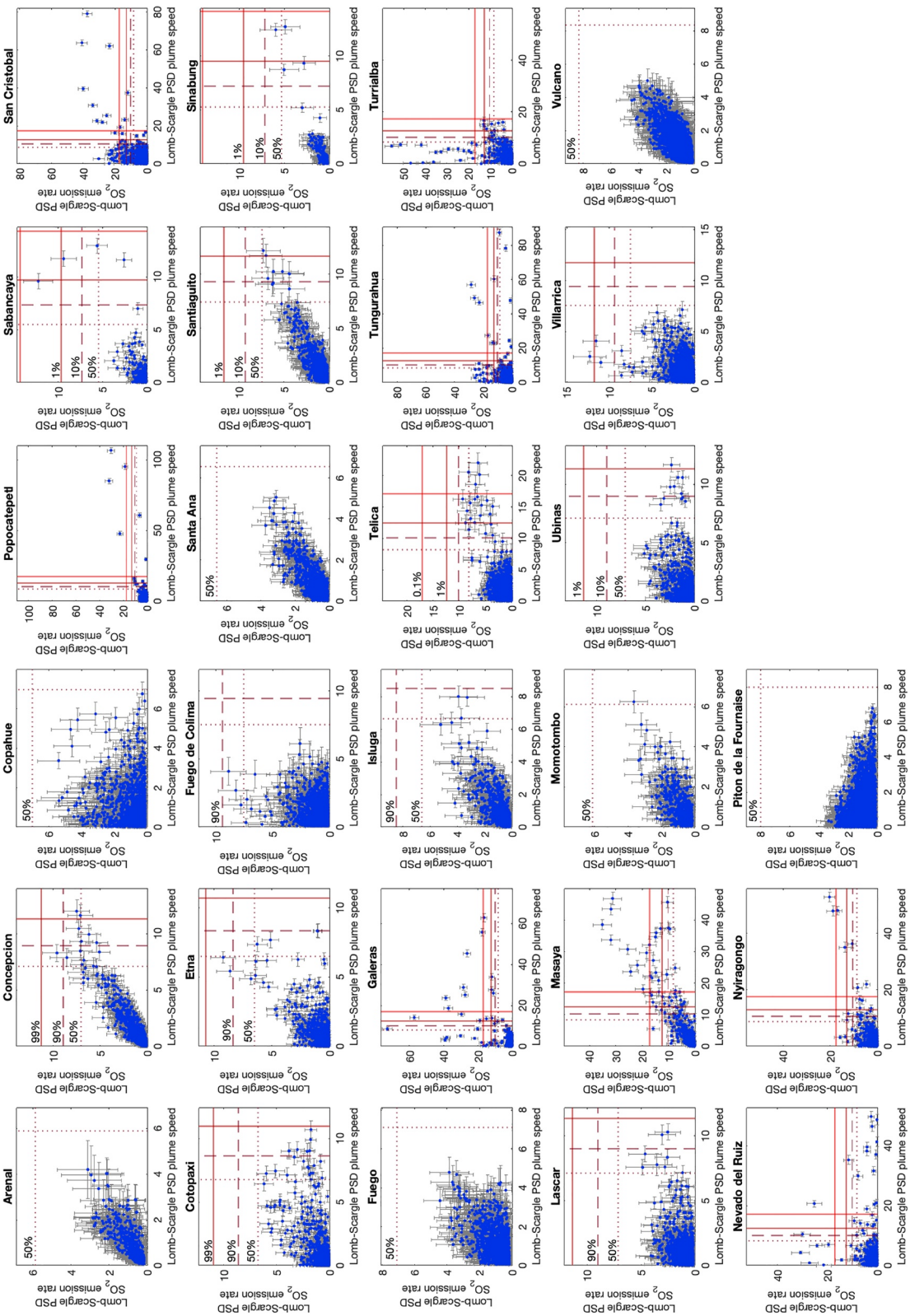

Figure 8. Lomb-Scargle Power Spectral Density (PSD) estimate of plume speed used to calculate SO_2 emission rate, and PSD estimate of SO_2 emission rate for periods between the pseudo-Nyquist frequency and $N/4$ for remaining volcanoes in the NOVAC Database. Datapoints are the median PSD estimate and error bars are the standard deviation. Horizontal and vertical lines represent the threshold values corresponding to FAPs of 50%, 10%, 1%, and 0.01%, see Table C1 for PSD threshold values associated with FAP at each volcano. Refer to Figure 6b for further explanation.

21699356, 2022, 12, Downloaded from https://agupubs.onlinelibrary.wiley.com/doi/10.1029/2022JB025380 by Cochrane France, Wiley Online Library on [05/01/2023]. See the Terms and Conditions (https://onlinelibrary.wiley.com/terms-and-conditions) on Wiley Online Library for rules of use; OA articles are governed by the applicable Creative Commons License

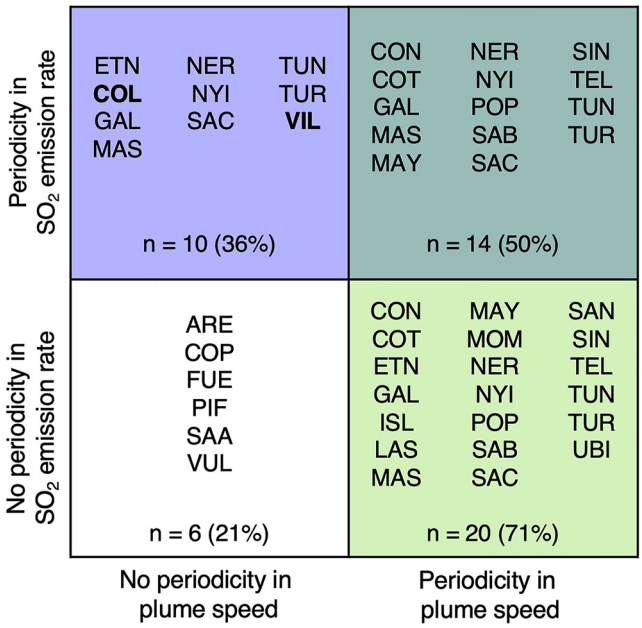

Figure 9. Relationships between the SO_2 emission rate and plume speed periodicities for all volcanoes. Groupings are not exclusive, so a volcano may feature in more than one group, except for the "no periodicity" category (white) which are volcanoes where statistically significant periodicities were not found in either the time series of SO_2 emission rate or plume speed. Volcanoes which *only* occupy the group where periodicities were found in the SO_2 emission rate and not in-plume speed are further distinguished in bold. Volcanoes are listed alphabetically where *n* is the number of volcanoes in each group, and the percentage of the total volcanoes studied is included in parenthesis. Code names are the same as those in Figure 1: ARE: Arenal, Costa; COL: Fuego de Colima, Mexico; CON: Concepción, Nicaragua; COP: Copahue, Chile-Argentina; COT: Cotopaxi, Ecuador; ETN: Etna, Italy; FUE: Fuego, Guatemala; GAL: Galeras, Colombia; ISL: Isluga, Chile-Bolivia; LAS: Lascar, Chile; MAS: Masaya, Nicaragua; MAY: Mayon, Philippines; MOM: Momotombo, Nicaragua; NER: Nevado del Ruiz, Colombia; NYI: Nyiragongo, Democratic Republic of the Congo; PIF: Piton de la Fournaise, France; POP: Popocatépetl, Mexico; SAB: Sabancaya, Peru; SAC: San Cristóbal, Nicaragua; SAA: Santa Ana, El Salvador; SAN: Santiaguito, Guatemala; SIN: Sinabung, Indonesia; TEL: Telica, Nicaragua; TUR: Turrialba, Costa Rica; TUN: Tungurahua, Ecuador; UBI: Ubinas, Peru; VIL: Villarrica, Chile; and VUL: Vulcano, Italy.

3.2.2. Common Causation for Periodicity in Wind Speed and Emissions of SO_2

It has been shown that ocean tides cause a dragging effect on the lower atmosphere (Renault & Marchesiello, 2022) and therefore suggests tidal forcing as a common cause for the periodicities observed in both wind speed and SO_2 emission rates. Renault and Marchesiello (2022) show transfer of moments from the principal lunar semidiurnal constituent (M_2) with a period of 12.42 hr produces tidal winds with amplitudes >1 m s^{-1} which could be particularly significant for determining SO_2 emission rates at volcanoes in coastal settings, such as Mayon. Although tidal winds associated with the M_2 constituent are shorter than the minimum periodicities detectable in the time series data used in this study, there exists several lower-amplitude, longer period tidal harmonics which have been linked to periodicities in the SO_2 emission rate at several volcanoes (Bredemeyer & Hansteen, 2014; Dinger et al., 2018; Girona et al., 2018). These include the lunar tidal constituents: lunar ter-monthly (M_{tm}), lunisolar synodic fortnightly (MS_{sf}), and lunisolar monthly (MS_m) tidal constituents with periods of ~9, ~15, and ~32 days, respectively, in addition to the fortnightly M_f tide. We show that zonal wind speeds at Mayon have periodicities at 14 (FAP 50%) and 28 days (FAP 0.1%) (Figure 7), these are not reflected in the PSD of SO_2 emission rate (Figure 4). Furthermore, the 51-day periodic trend in the SO_2 emission rate at Mayon volcano cannot be explained by ocean tides. To our knowledge, there is no evidence for large amplitude, long period tidal constituents which may satisfy common periodicities in both wind speed and SO_2 emission rates we identify at several volcanoes (Figure C1).

3.2.3. Systematic Influence of Wind Speed on Downwind Measurements of SO_2 Emission Rate

While we dismiss any direct causal link between wind speed and volcanic degassing, we may consider the influence of wind speed on downwind measurements of SO_2 emissions. According to Bernoulli's principle, a low-pressure zone will form as strong horizontal winds blow across the volcanic summit. If volcanic gases typically accumulate in the crater, the resulting pressure difference will produce an upward lifting force releasing the accumulated gas and causing a perceived increase in the SO_2 emission rate as it is measured downwind. However, the dynamic pressure will normally be too small to contribute significantly to change the emission. Winds may however perturb a stagnant air mass that has equilibrated inside a depression such as a crater, forcing convection by turbulence. A similar effect is well documented in the diffuse emission of CO_2 at several volcanoes (Laiolo et al., 2016; Lewicki et al., 2007; Viveiros et al., 2008, 2015). Soil CO_2 fluxes from Furnas and Fogo volcanos (São Miguel Island, Azores) vary with local barometric pressure and wind speed (Viveiros et al., 2008, 2015) while weather fronts with strong winds influence gas flow in the near-surface environment at Mammoth Mountain, USA (Lewicki et al., 2007). These examples highlight the influence of meteorology, specifically wind speed, on measured emission rates of volcanic gases.

Gas accumulation in the crater has been proposed to account for correlations between wind speed and SO_2 emission rate at Masaya volcano (Dinger et al., 2021), but it seems unlikely that it could account for the common periodicities identified here, owing to the range of volcano types and surface activity. Despite explosive emissions creating poor measurement conditions, SO_2 emission rates used in this study span episodes of both explosive activity and passive degassing (Figure A1). Several volcanoes where periodicities in the SO_2 emission rate have been identified were in eruption (active degassing) for the complete (e.g., Sinabung) or part (e.g., Nevado del Ruiz, Nyiragongo) duration of the time series used in this study (GVP, 2013a). We therefore expect initial plume conditions were driven by volcano processes rather than buoyancy due to atmospheric conditions, making it

21699356, 2022, 12, Downloaded from https://agupubs.onlinelibrary.wiley.com/doi/10.1029/2022JB025380 by Cochrane France, Wiley Online Library on [05/01/2023]. See the Terms and Conditions (https://onlinelibrary.wiley.com/terms-and-conditions) on Wiley Online Library for rules of use; OA articles are governed by the applicable Creative Commons License

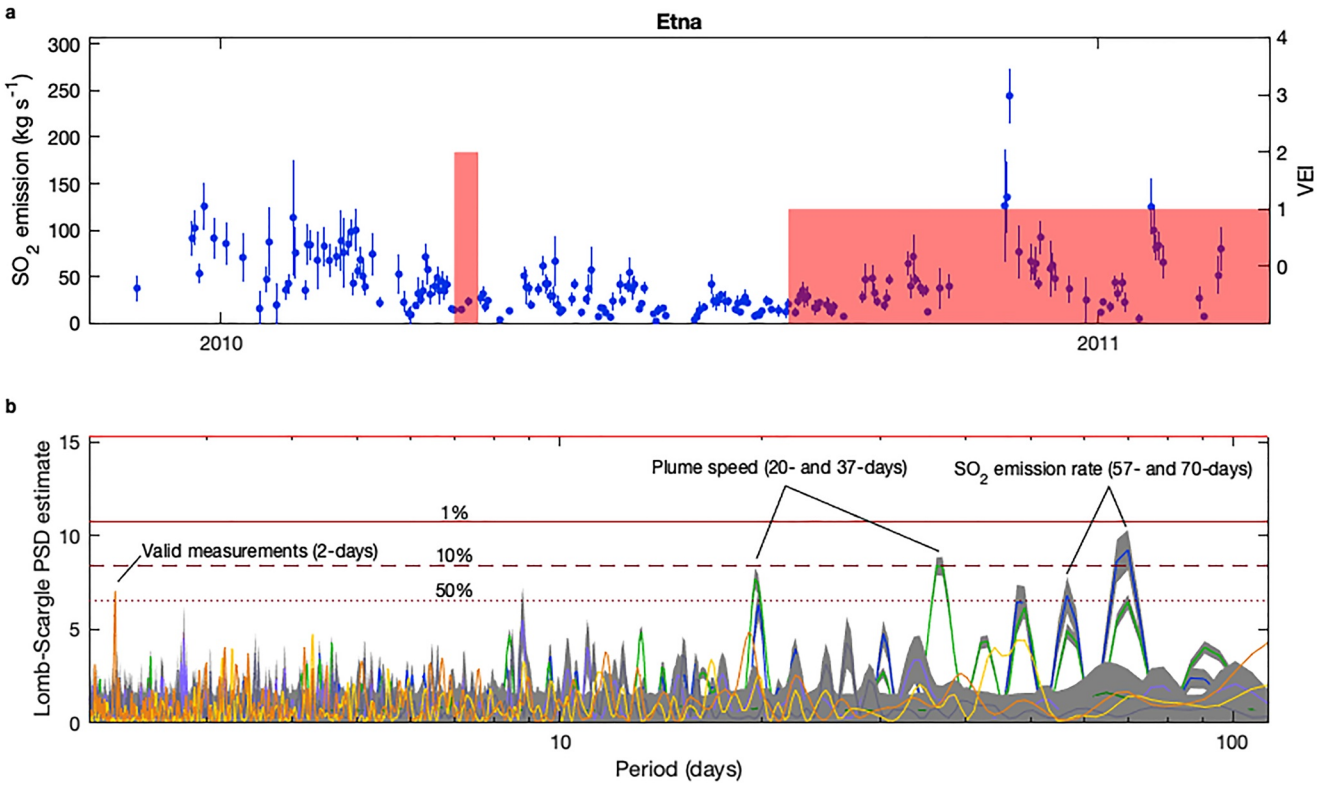

Figure 10. Emission rate of SO_2 for Etna volcano with periodicities in SO_2 emission unaccompanied by statistically significant periodicities in wind speed. (a) Daily mean SO_2 emission rates are plotted as blue circles and error bars are the standard deviation (Salerno et al., 2020). Eruptive activity is shown by red bars, according to the Smithsonian's Global Volcanism Program database (Global Volcanism Project, 2013a). Where no eruption end date is listed, 10-days is used by default, unless it is the most recent entry and therefore is considered an ongoing eruption. (b) Lomb-Scargle Power Spectral Density (PSD) estimate of SO_2 emission and PSD of parameters used to determine SO_2 emission rate at Etna volcano, at periods between the pseudo-Nyquist frequency (2 days) and *N*/4 (133 days). Median PSD estimates for each parameter are shown as single solid lines and corresponding standard deviation is shown in gray. Colors refer to the following parameters: SO_2 emission rate (blue), plume speed (light green), plume direction (dark green), distance to plume (magenta), plume width (lilac), cloud cover (gray), total measurements (yellow), and valid measurements (orange). Horizontal lines correspond to False Alarm Probability (FAP) of 50%, 10%, 1%, and 0.01% (where some labels have been omitted for readability), see Table C1 for PSD threshold values associated with FAP at each volcano. Statistically significant periodicities are labeled.

unlikely that gas accumulation could be responsible for the identified periodicities. Furthermore, several volcanoes have undergone changes to their summit morphology during this time and/or have craters that are unfavorable for gas accumulation. For the case of Mayon volcano, a summit lava dome appeared in August 2014 and occupied a large part of the summit crater, which is breached to the south. As corroborated by visual observations, significant gas accumulation in the crater is unlikely. These considerations point to the turbulence effect as an unlikely source for a systematic influence on measurements of SO_2 emission rate.

Another possibility is an observational bias relating to our inability to accurately quantify SO_2 emission rates depending on characteristics of the plume. Concentrated, narrow plumes, formed by strong winds, are more straightforward to measure compared to dispersed plumes which contain more entrained atmospheric air and typically lower SCDs of SO_2 (Lübcke et al., 2016). Variations in plume buoyancy and subsequently plume height may also affect our ability to accurately quantify SO_2 emission rate. In certain topographic conditions, strong winds may cause a loss of altitude in the plume as it is transported downwind, which may influence the possibility to measure the plume by the scanning method. In this case, SO_2 emission rates determined from scanning instruments will be subject to sampling bias depending on the value of the wind. By preforming our analysis on all parameters, we attempt to account for periodicities arising from observational bias but note that for some volcanoes, including Mayon, owing to the location of the instruments, it is not possible to constrain plume height by triangulation of two scans. In this case, the plume height is assumed to be constant at summit altitude which may signify windspeed as an indirect cause of periodicities in the time series of SO_2 emission rate. We find however no evidence of periodicity in the plume height parameter in the time series where it has been calculated (Figure D1). Observational bias is an important consideration for networks with reduced instrument coverage

21699356, 2022, 12, Downloaded from https://agupubs.onlinelibrary.wiley.com/doi/10.1029/2022JB025380 by Cochrane France, Wiley Online Library on [05/01/2023]. See the Terms and Conditions (https://onlinelibrary.wiley.com/terms-and-conditions) on Wiley Online Library for rules of use; OA articles are governed by the applicable Creative Commons License

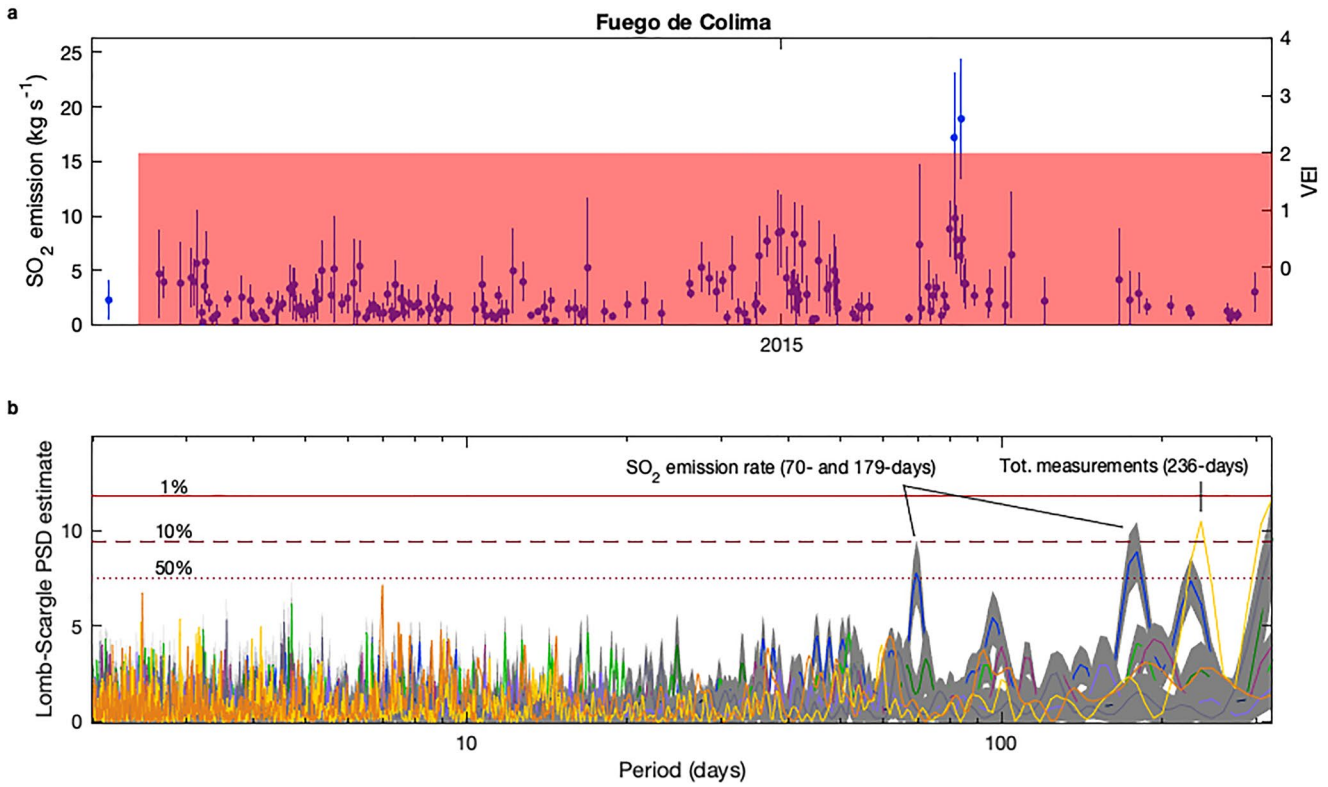

Figure 11. Emission rate of SO_2 for Fuego de Colima volcano with periodicities in SO_2 emission unaccompanied by statistically significant periodicities in wind speed. (a) Daily mean SO_2 emission rates are plotted as blue circles and error bars are the standard deviation (Delgado et al., 2020a). Eruptive activity is shown by red bars, according to the Smithsonian's Global Volcanism Program database (Global Volcanism Project, 2013a). Where no eruption end date is listed, 10 days is used by default, unless it is the most recent entry and therefore is considered an ongoing eruption. (b) Lomb-Scargle Power Spectral Density (PSD) estimate of SO_2 emission and PSD of parameters used to determine SO_2 emission rate at Fuego de Colima, at periods between the pseudo-Nyquist frequency (2 days) and $N/4$ (323 days). Median PSD estimates for each parameter are shown as single solid lines and corresponding standard deviation is shown in gray. Colors refer to the following parameters: SO_2 emission rate (blue), plume speed (light green), plume direction (dark green), plume altitude (navy), distance to plume (magenta), plume width (lilac), cloud cover (gray), total measurements (yellow), and valid measurements (orange). Horizontal lines correspond to False Alarm Probability (FAP) of 50%, 10%, 1%, and 0.01% (where some labels have been omitted for readability), see Table C1 for PSD threshold values associated with FAP at each volcano. Statistically significant periodicities are labeled.

although we demonstrate a lack of observational bias in reported SO_2 emissions at Mayon with the absence of periodicities which are identified in the plume direction and distance to plume (Figure 5). Longer periods are identified in other parameters, particularly total number of measurements and the distance to plume, but the periodicities in SO_2 emissions rate at Mayon, and several other volcanoes (e.g., Etna, Fuego de Colima) are unaccompanied by periodicities in additional parameters other than plume speed. Although the ICA of SO_2 that is measured is expected to vary as a function of plume speed (in the case of constant emission rate), comparing the time series of ICA with plume speed may offer straightforward means to investigate observational biases further.

3.2.4. Systematic Error in the Plume Speed Used to Derive SO_2 Emission Rates

For measurements conducted under ideal conditions, it is well-known that plume speeds are the main source of error in SO_2 emission rates (Arellano et al., 2021) and correlations have been observed between SO_2 emission rate and wind speed at several volcanoes (e.g., Dinger et al., 2021). The fact that these correlations translate into periodicities implies a systematic error in the calculation of SO_2 emission rates. A simple rationale would be the limitation in using wind speeds derived from the ECMWF ERA-Interim database to accurately represent plume velocity.

Oversimplified representation of complex topography has been proposed to explain the differences between ECMWF ERA-Interim data and observations of surface conditions (e.g., Luo et al., 2019; Mengistu Tsidu et al., 2015; Posada-Marin et al., 2019; Wang et al., 2015). When air flow is met by orographic barriers, such as a mountain ranges, the air is forced to flow over the high topography or divert around it (Helbig et al., 2017;

21699356, 2022, 12, Downloaded from https://agupubs.onlinelibrary.wiley.com/doi/10.1029/2022JB025380 by Cochrane France, Wiley Online Library on [05/01/2023]. See the Terms and Conditions (https://onlinelibrary.wiley.com/terms-and-conditions) on Wiley Online Library for rules of use; OA articles are governed by the applicable Creative Commons License

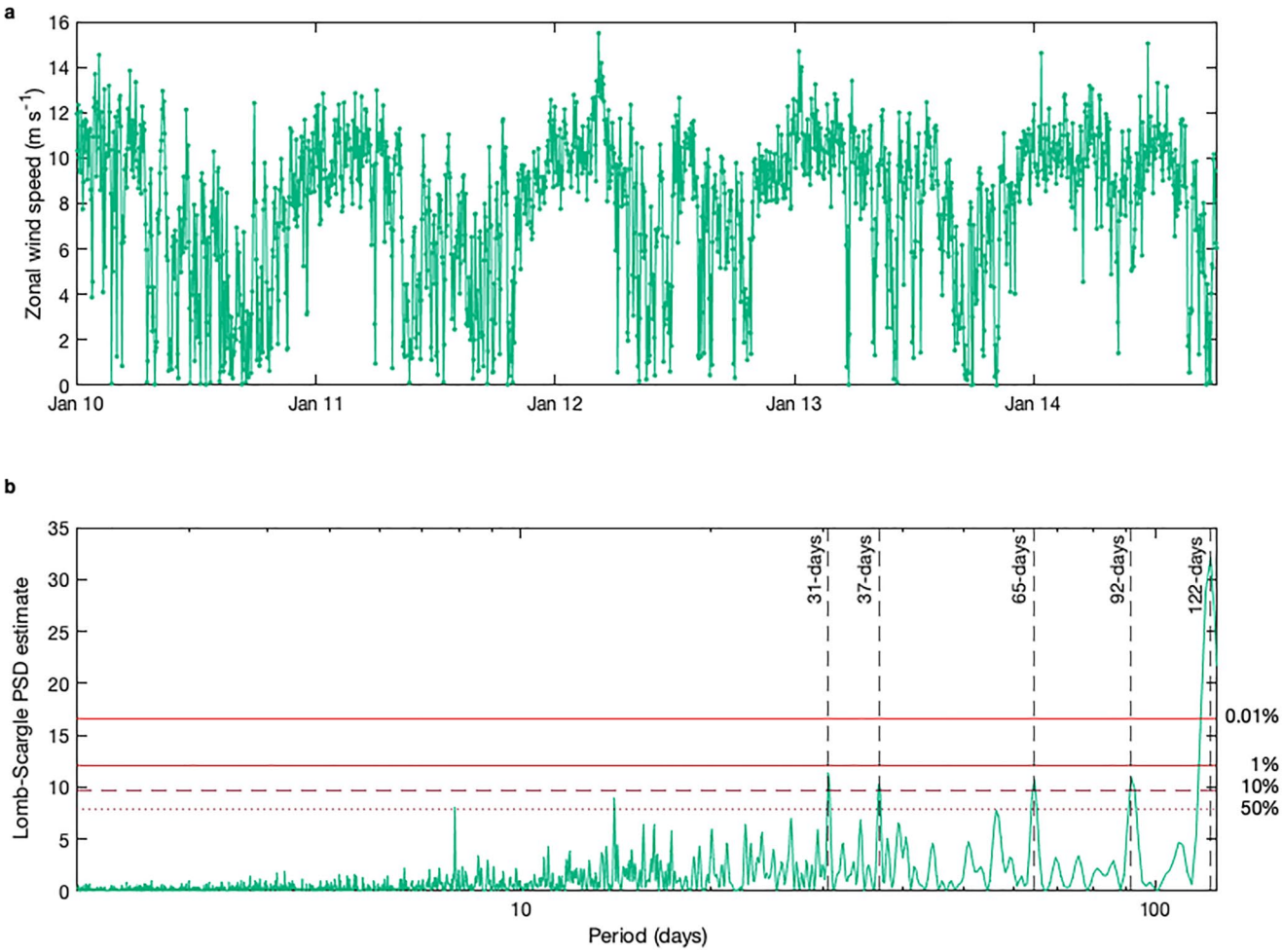

Figure 12. (a) Continuous time series of the magnitude of zonal wind component at Masaya volcano. Atmospheric specifications are provided by the European Centre for Medium-Range Weather Forecasts (ECMWF, 2022) operational High spatial RESolution forecasts (HRES) products with 137 levels (cycle 38r2). Wind speed information is extracted for the latitude and longitude closest to Masaya volcano (12.0°N and 86.2°W) and atmospheric level closest to the plume altitude used for determining SO_2 emission rate (460 m asl). (b) Lomb-Scargle Power Spectral Density (PSD) estimate of zonal wind speeds. Horizontal lines correspond to False Alarm Probability (FAP): 50% (7.8), 10% (9.7), 1% (12.1), and 0.01% (16.7). Vertical solid lines indicate the periodicities identified which have FAP < 10%, enabling rejection of the null hypothesis with >90% confidence. Several additional peaks in PSD with FAP < 50% are also apparent.

Rotach et al., 2015). The same happens for small-scale orographic features, such as hills or ridges. Volcanic regions are typically characterized by complex topography, particularly stratovolcanoes, which generate prominent orographic features and may act as wind barriers. Favalli et al. (2004) found winds hitting Mount Etna's flanks were met by strong sea breeze, which resulted in the formation of convective currents and found that measured wind speeds were 2.5 times greater than the in-plume speeds calculated by numerical modeling. Reduced wind speeds on the leeward side of the volcano are often observable, when the plume appears stationary, hugging the flank (e.g., Bluth et al., 2007). Nadeau and Williams-Jones (2009) discuss topographic modification of winds at Masaya volcano, where an apparent loss of SO_2 with distance downwind, is thought to relate to local variations in wind speed. Orographic acceleration (Oke, 1987) of winds over a topographic ridge causes localized dilution of the plume in the direction which it travels. By converting the lower concentration of measured SO_2 to an emission rate using a single plume speed, SO_2 emission rates are underestimated (Nadeau & Williams-Jones, 2009). Alternative wind models are increasingly being used to improve the accuracy of SO_2 emission rates (e.g., Hidalgo et al., 2018), including the Weather Research and Forecasting (WRF) Model owing to its higher resolution over complex terrain (Powers et al., 2017). Leeward wind conditions, however, remain challenging to predict (Bao et al., 2018; Bechmann et al., 2011). Instruments belonging to the NOVAC network are deliberately placed 5–10 km downwind in order to minimize topographic effects due to the volcano edifice, although additional

21699356, 2022, 12, Downloaded from https://agupubs.onlinelibrary.wiley.com/doi/10.1029/2022JB025380 by Cochrane France, Wiley Online Library on [05/01/2023]. See the Terms and Conditions (https://onlinelibrary.wiley.com/terms-and-conditions) on Wiley Online Library for rules of use; OA articles are governed by the applicable Creative Commons License

21699356, 2022, 12, Downloaded from https://agupubs.onlinelibrary.wiley.com/doi/10.1029/2022JB025380 by Cochrane France, Wiley Online Library on [05/01/2023]. See the Terms and Conditions (https://onlinelibrary.wiley.com/terms-and-conditions) on Wiley Online Library for rules of use; OA articles are governed by the applicable Creative Commons License

topographic features, plume height and ambient atmospheric conditions in between may play a role. These complexities highlight the impact of topography on wind speed is underestimated and likely causing a significant error on derived emission rates of SO_2. Unless high resolution wind data, which can account for localized topographic effects, are used, the same effect will occur when using wind sources other than the ECMWF.

Overcoming uncertainty in the wind speed remains a major challenge for the accurate quantification of SO_2 emissions, since the measurement of SO_2 itself is a function of plume speed. One improvement may be to use the ICA of SO_2 together with the time series of plume speed. If the trend in-plume speed changes without an accompanying adjustment in the measured ICA, the disparity may reflect a change in degassing rate rather than atmospheric dynamics. The contribution of this study is to demonstrate that the dependencies between wind speed and SO_2 emissions rate translate into periodicities, but further work is needed to understand the magnitude of this effect. Given that the NOVAC Database contains substantial data on SO_2 emissions which have been determined with standardized methodology, this data may be used to identify the range of SO_2 emissions which are derived under and given atmospheric conditions. It may be advantageous to provide a quantitative statement which refers to the parameters used to derive the reported SO_2 emission rate. Providing passive degassing is the prominent state, considering percentile information of SO_2 emissions for any particular wind speed, e.g., may enable greater understanding as to whether fluctuations in SO_2 emission rate are due to changes in volcanic degassing or due to inaccuracies in-plume speed.

3.3. Previous Works on Periodicities of Volcanic Degassing

Previous studies of SO_2 emission rate at various volcanoes have identified several periodicities. For example, Pering et al. (2019) found multiple periodicities of 46, 94, 121, and 140 days in the emission rate of SO_2 at Masaya volcano determined using the same modeled wind speeds taken from the ECMWF ERA-Interim database (Dee et al., 2011) and suggested that these could be linked to cycles of magma replenishment. Our analysis of SO_2 emission rates between April 2007 and October 2014 shows a cluster of statistically significant periodicities between 83 and 185 days, the most significant at 137 days (FAP < 0.01%; Figure C1). Notwithstanding we also found that most periodicities in SO_2 emission rate are associated with periodicities in the plume speed (Figure 8 and Appendix D). Analysis of the continuous time series of zonal wind speeds at Masaya for 2010–2014 indicate periodicities at 31 and 37 days as well as 65, 92, and 122 days (Figure 12). Thus, the dynamics of global trade winds at this latitude may be an alternative explanation for the 94-day and 121-day periodicities previously found in SO_2 emission rates at Masaya. The absence of significant periodicities <∼80 days in the SO_2 emission rate we found suggests that the periodicities identified by Pering et al. (2019) begin after October 2014 may be a shift in the volcanic system. Alternatively, these periodic trends may not have been sufficiently significant to reach the 50% FAP threshold considering the longer periodicities we identify (Appendix B) or inclusion of the standard deviation in daily SO_2 emission rate.

Numerous periodicities have been identified in the emission rate of SO_2 from ground-based instruments at SHV (Montserrat): 8, 12, 19, 54, 150, 171, 730 days (Christopher et al., 2015; Nicholson et al., 2013). Several periodicities have also been identified in the time series of SO_2 mass measured by the Ozone Monitoring Instrument (OMI) onboard the Aura satellite: 7–8, 12, 54–58, 102, 121, 159 days (Flower & Carn, 2015). While the 7–8-day cycle is thought to result from the orbital characteristics of the Aura satellite, others periodicities also correspond to those identified in the time series of geophysical parameters (Nicholson et al., 2013). Longer period cycles at ∼55, ∼102, ∼121, and ∼159 days have been linked to the volcanic system and with magma ascent and/or pulsatory magma injection (Christopher et al., 2015; Flower & Carn, 2015). We did not analyze data from SHV, but given that it is located at a similar latitude of Masaya and Mayon it may be possible that the MJO regulates wind speeds with similar periodicities to those found at SHV. Variability of the Caribbean low-level jet acts to strengthen or weaken low-level winds and is subject to phases of the MJO, producing semiannual and interannual variability in zonal winds (Martin & Schumacher, 2011; Muñoz et al., 2008). Wind speeds are not used to derive emission rates from data acquired by OMI, but the mass of SO_2, or more importantly its distribution, is a function of wind speed (Nadeau & Williams-Jones, 2009). Meteorological influence has been ruled out as the source of a 159-day period at Soufriere Hills, but only variability in cloud cover is considered (Flower & Carn, 2015). Wind speeds have been suggested as a source for unexplained periodicities in SO_2 emission rates (4 and 16 days) derived from OMI at Redoubt volcano (USA, Lopez et al., 2013). Although Lopez et al. (2013) highlight the

21699356, 2022, 12, Downloaded from https://agupubs.onlinelibrary.wiley.com/doi/10.1029/2022JB025380 by Cochrane France, Wiley Online Library on [05/01/2023]. See the Terms and Conditions (https://onlinelibrary.wiley.com/terms-and-conditions) on Wiley Online Library for rules of use; OA articles are governed by the applicable Creative Commons License

16 days repeat cycle of the Aura satellite we also note the potential for short-term periodic trends in wind speeds, as we found a 16-day periodicity (0.01% FAP) in the zonal wind speeds at Mayon (Figure 7).

Wind speed dynamics provide an alternative explanation for the periodic trends in SO_2 emission rates but cannot explain the periodicities reported in geophysical data sets. For example, the periodicities of ∼50 days at SHV in both SO_2 emission rate and seismic data imply a common volcanic origin (Lamb et al., 2014). A 10–14-day period in the time series of reported SO_2 emission rates was previously found at Turrialba (Costa Rica) which correspond to cycles in time series of Real-time Seismic Amplitude Measurements (RSAM) and tremor (Conde et al., 2014). We did not identify a significant periodicity in SO_2 emission rate at Turrialba, but we identify a 12-day periodicity (FAP 10%) in the number of valid measurements contributing to the reported daily SO_2 emission. Lamb et al. (2014) found a 71-day periodicity (>95% confidence level) in low-amplitude long period events at Fuego de Colima (Mexico) during 2006 and 2011. Our analysis of SO_2 emission rates between 2013 and 2016 indicate a 70-day periodicity (50% FAP) which was not obviously related to any other parameter we analyzed (Figure 11) and may therefore be volcanic in origin. We also find a 170-day periodicity (50% FAP) for which a periodic trend in seismic data is not apparent (Lamb et al., 2014).

Several studies have reported an influence of the fortnightly (∼13.7 days) Earth tides on volcanic degassing (Bredemeyer & Hansteen, 2014; Conde et al., 2014; Dinger et al., 2018). Despite time series of SO_2 emission rates being incomplete, we demonstrate the possibility to detect periodicities in the order of 14 days using synthetic spectra (Appendix B). We did not find evidence for the influence of Earth tides on the emission rate of SO_2 from volcanoes included in the NOVAC network. It is possible that periodicities related to the dominant tidal components are present, but they may be far less pronounced compared with the intraannual and interannual periodicities we identified. Most time series used in this study are multiyear in duration (Figure A1). Multiple PSD peaks in close proximity are unlikely to represent discrete periodic trends, rather the variability of a single periodic component. FAP provide a measure of the probability that the returned PSD may be produced by randomly distributed data. A 14-day periodic trend which is present for a short period of time is more likely to be caused by randomly distributed data than if occurring over multiple years (assuming equivalent noise). Therefore, it is unlikely that we would find statistically significant periodicities due to Earth tides if they are transient, rather than continuous. Notwithstanding, the PSD estimates corresponding to ∼14 days are notably low for several volcanoes where the influence of Earth tides has been suggested (e.g., Mayon, Turrialba, Villarrica; Bredemeyer & Hansteen, 2014; Conde et al., 2014; Ramos et al., 1985). Both complete time series of ECMWF ERA-Interim data we analyzed identify ∼7-day and ∼14-day periodicities in zonal wind speeds (∼7 and 16 days at Mayon and 8 and 14 days at Masaya) which coincide with tidal components.

4. Conclusions and Future Work

We have identified significant periodicities in the SO_2 emission rates in 17 out of the 28 volcanoes included in the NOVAC Database. About 50% of the volcanoes analyzed show significant correlation between periodicities in SO_2 emission rate and the plume speed used to derive emission rates. Ten volcanoes (36% of the total) appear to show periodicities in SO_2 emission rate that are unaccompanied by periodicities in-plume speed. However, detailed inspection of all parameters involved in determining the SO_2 emission rates show that only those from Fuego de Colima volcano may be of magmatic origin. For all other volcanoes, periodicities in SO_2 emission rate are associated with periodicities in-plume speed or other parameters. Periodicities occur at about 30–70, ∼120, and ∼180 days in SO_2 emission rate and these appear to be related to the intraseasonality and interseasonality in global trade winds. Specifically, those between 30 and 70 days likely relate to variation in wind speed according to the Madden-Julian Oscillation.

Our findings show SO_2 emission rates and the wind speed used to derive them have common periodicities. We do not find a common causation between wind speed and SO_2 degassing and thus we suggest that there is a systematic bias in the calculation of SO_2 emission rates. Inaccuracies may arise due to the limitation of using wind speeds derived from the ECMWF ERA-Interim database but may also occur when the wind speed data are of limited temporal or spatial resolution to accurately represent plume velocity at the measurement time and location. This highlights the critical importance of having accurate wind data for deriving realistic SO_2 emissions, particularly when identifying periodic trends related to volcanic behavior. Some volcano observatories derive more accurate SO_2 emission rates using representative wind data for the purpose of volcano monitoring. To avoid the assumption that the apparent periodicities relate to the magmatic system, analysis should also be performed

on the parameters used to derive SO_2 emission rates which may offer opportunity to improve measurements of SO_2 emissions from volcanoes. To mitigate against the effects of inaccuracies in wind speed, we suggest to remove the periodic trends in the time series of SO_2 emission rate which are also present in the wind speed. By removing these long-term periodicities, it may be possible to capture more subtle variations in SO_2 emission rate related to magmatic processes. In addition, owing to the large uncertainties, incorporating the standard deviation of reported SO_2 emission rates is necessary. Finally, contrary to several studies, we find no statistically significant periodicities related to the long-term influence of Earth tides on volcanic degassing of SO_2.

Appendix A: SO_2 Emission Rate for Volcanoes Included in the NOVAC Database

Figure A1shows the times series of SO_2 emission rate for all volcanoes included in the NOVAC Database and considered in this study.

21699356, 2022, 12, Downloaded from https://agupubs.onlinelibrary.wiley.com/doi/10.1029/2022JB025380 by Cochrane France, Wiley Online Library on [05/01/2023]. See the Terms and Conditions (https://onlinelibrary.wiley.com/terms-and-conditions) on Wiley Online Library for rules of use; OA articles are governed by the applicable Creative Commons License

10.1029/2022JB025380

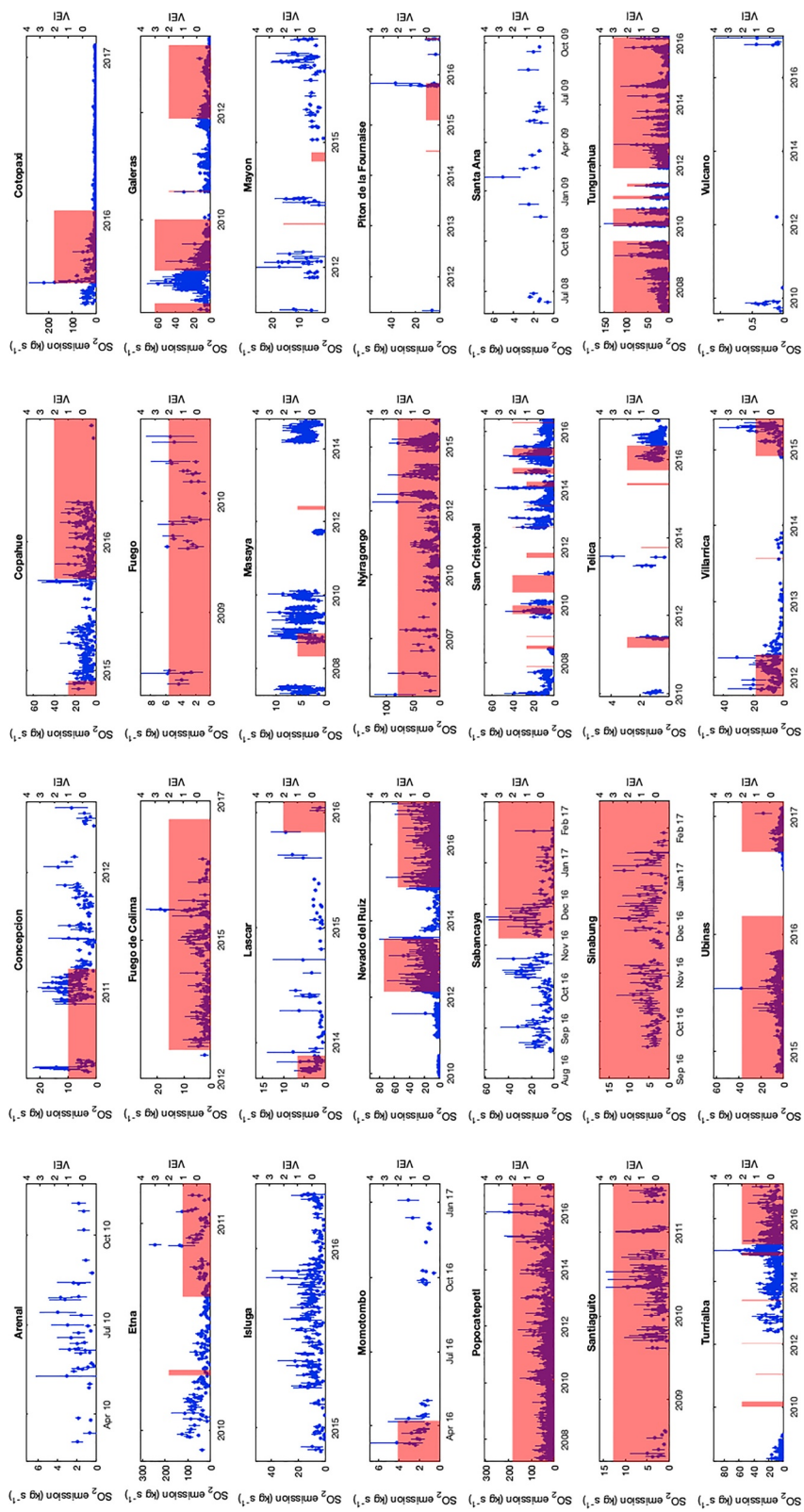

Figure A1. Daily mean SO_2 emission rates are plotted as blue circles and error bars represent the corresponding standard deviation. Eruptive activity is represented by red bars, using confirmed eruptions as defined in the Smithsonian's Global Volcanism Program database (Global Volcanism Project, 2013a). Where no eruption end date is listed, 10 days is used by default, unless it represents the most recent entry and therefore is considered an ongoing eruption. No data are presented for Llaima, Planchón-Peteroa, Sangay, and San Miguel volcanoes, since the minimum number of datapoints (8) was not satisfied. Data presented here are taken from the NOVAC Database: Arenal (Avard et al., 2020); Concepción (Saballos et al., 2020a); Copahue (Velasquez et al., 2020a); Cotopaxi (Hidalgo et al., 2020a); Etna (Salerno et al., 2020); Fuego de Colima (Delgado et al., 2020a); Fuego (Gustavo Chigna et al., 2020a); Galeras (Chacon et al., 2020a); Isluga (Bucarey et al., 2020a); Lascar (Bucarey et al., 2020b); Masaya (Saballos et al., 2020b); Mayon (Bornas et al., 2020); Momotombo (Saballos et al., 2020c); Nevado del Ruiz (Chacon et al., 2020b); Nyiragongo (Yalire et al., 2020); Piton de la Fournaise (DiMuro et al., 2020); Popocatépetl (Delgado et al., 2020b); Sabancaya (Masias et al., 2020a); San Cristóbal (Saballos et al., 2020d); Santa Ana (Montalvo et al., 2020); Santiaguito (Chigna et al., 2020b); Sinabung (Kasbani et al., 2020); Telica (Saballos et al., 2020e); Tungurahua (Hidalgo et al., 2020b); Turrialba (Avard, Galle, & Arellano, 2020); Ubinas (Masias et al., 2020b); Villarrica (Velasquez et al., 2020b); and Vulcano (Vita et al., 2020).

21699356, 2022, 12, Downloaded from https://agupubs.onlinelibrary.wiley.com/doi/10.1029/2022JB025380 by Cochrane France, Wiley Online Library on [05/01/2023]. See the Terms and Conditions (https://onlinelibrary.wiley.com/terms-and-conditions) on Wiley Online Library for rules of use; OA articles are governed by the applicable Creative Commons License

21699356, 2022, 12, Downloaded from https://agupubs.onlinelibrary.wiley.com/doi/10.1029/2022JB025380 by Cochrane France, Wiley Online Library on [05/01/2023]. See the Terms and Conditions (https://onlinelibrary.wiley.com/terms-and-conditions) on Wiley Online Library for rules of use; OA articles are governed by the applicable Creative Commons License

Appendix B: Lomb-Scargle PSD Estimate of Synthetic Signals

B1. Datagaps and Noise

To test the methods used in this study, we applied the Lomb-Scargle approach to several synthetic signals with known periodicities. We rescaled and resampled a 50-day periodic signal to match the magnitude of SO_2 emission rates and days for which an SO_2 emission rate is available at Mayon. We prepared a second synthetic signal but this time adding noise (Figure B1), before plotting the Lomb-Scargle periodogram of each signal (Figure B2). Despite the large datagaps which exist in the time series data at Mayon, the Lomb-Scargle approach identifies a clear peak in the PSD estimates at 50 days (Figure B2a). Several noticeable peaks surround the 50-day peak, at about half the maximum PSD estimate, however. Figure B2b reveals the effect of noise on the Lomb-Scargle periodogram. While the periodogram appears similar to that obtained in Figure B2a the magnitude 50-day peak is reduced (now 13 compared to 46). Despite the reduction in PSD estimate, the peak at 50 days remains pronounced.

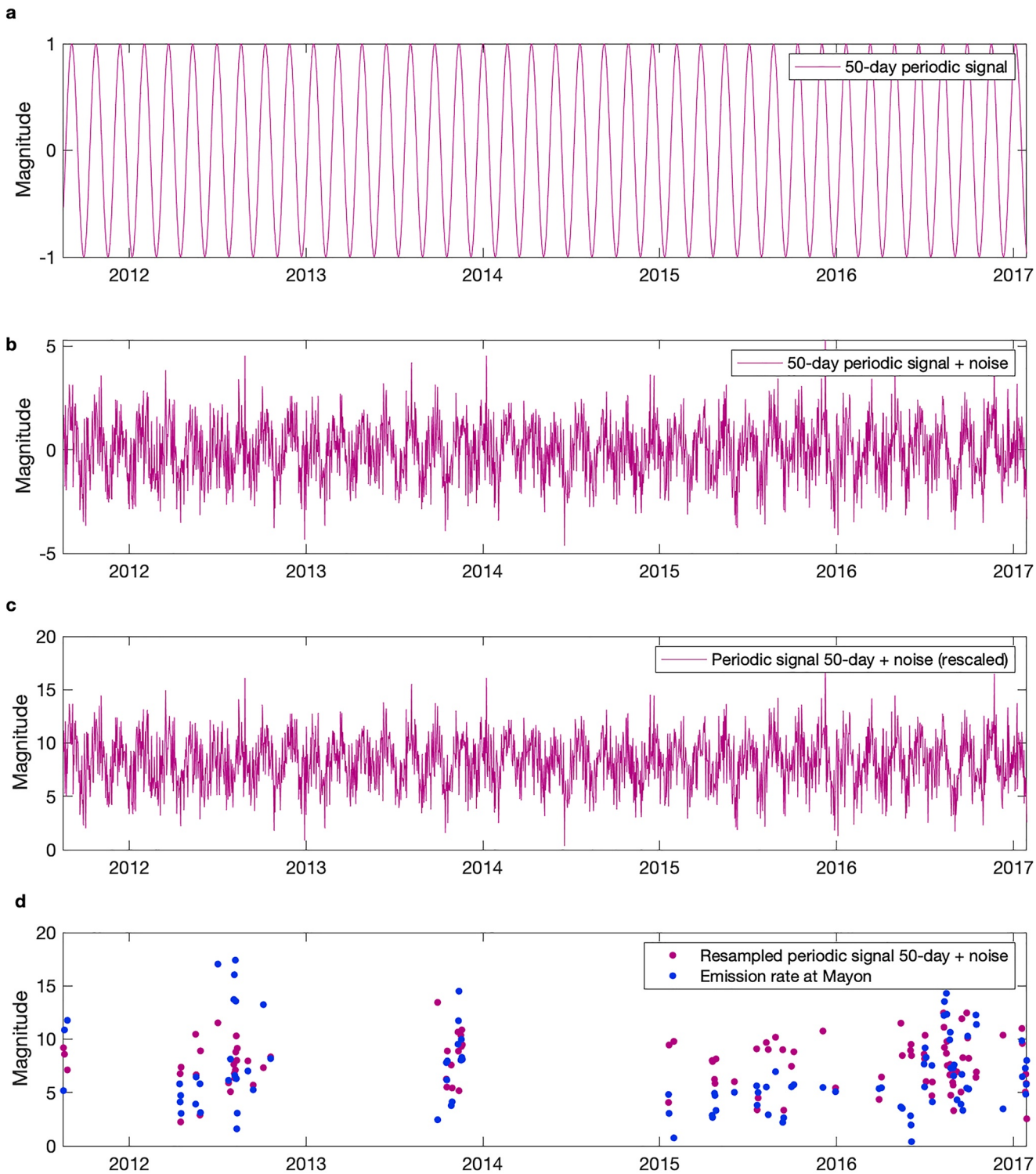

Figure B1. (a) Synthetic signal with 50-day periodicity. (b) Noise was added to the synthetic signal using MATLAB function "aywgn" (MathWorks, 2021). We used "measurement" and "linear" as function inputs to measure the power of the synthetic signal and apply Gaussian noise equivalent to the *snr* at Mayon. We define the *snr* as the mean of daily standard deviation divided by the daily SO_2 emission rate (0.37). (c) The noisy synthetic signal is rescaled to match the magnitude of SO_2 emission rates reported at Mayon volcano and (d) resampled to match the days for which an SO_2 emission rate is available at Mayon volcano.

21699356, 2022, 12, Downloaded from https://agupubs.onlinelibrary.wiley.com/doi/10.1029/2022JB025380 by Cochrane France, Wiley Online Library on [05/01/2023]. See the Terms and Conditions (https://onlinelibrary.wiley.com/terms-and-conditions) on Wiley Online Library for rules of use; OA articles are governed by the applicable Creative Commons License

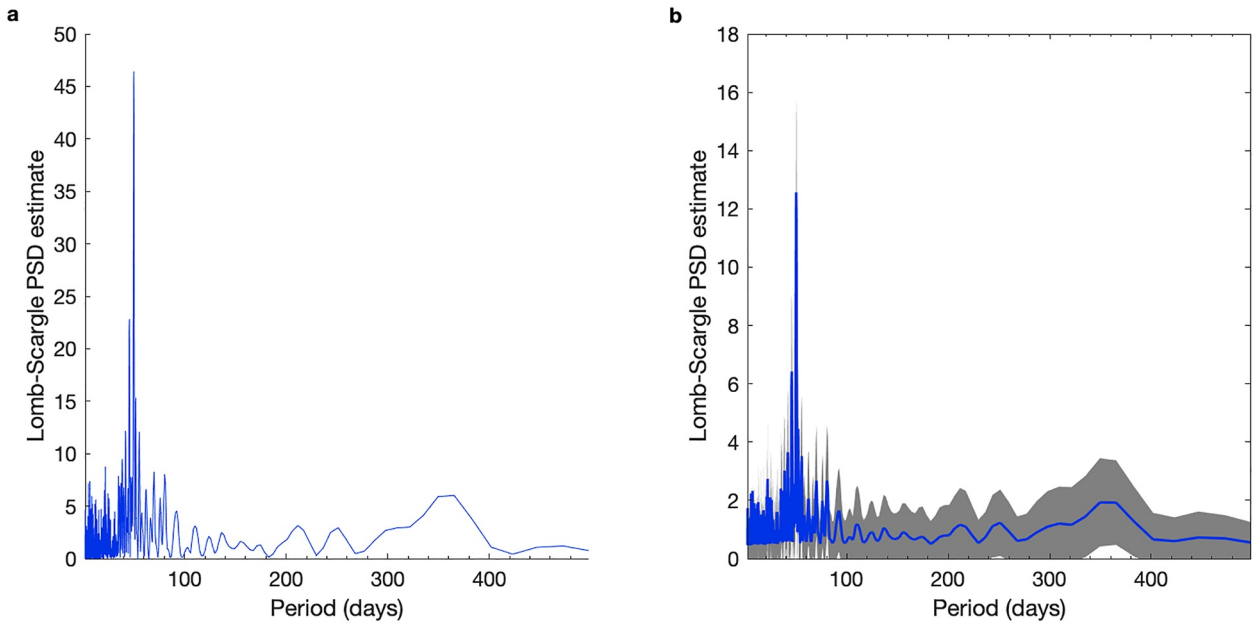

Figure B2. (a) Lomb-Scargle Power Spectral Density (PSD) estimate of 50-day periodic signal in Figure B1a which has been rescaled and resampled to match the magnitude of SO_2 emission rates reported and resampled to match the days for which an SO_2 emission rate is available at Mayon. (b) Median (blue line) and standard deviation (gray shaded) of Lomb-Scargle PSD estimates from 1,000 signals all with 50-day periodic trend but with different Gaussian noise applied (as in Figure B1b). Signals were scaled and resampled to match the magnitude of SO_2 emission rates reported and the days for which an SO_2 emission rate is available at Mayon volcano.

B2. FAPs

We use FAPs to determine which peaks in the PSD estimate are significant. To validate the use of FAPs in our approach, we calculate Lomb-Scargle PSD estimates of 1,000 signals comprised purely of Gaussian noise and calculated FAPs of 50%, 10%, 1%, and 0.01% (Figure B3). None of the signals returned PSD estimates which reached the 0.01% FAP threshold. Only six signals (0.6%) returned PSD estimates that reached the 1% FAP threshold, 7 signals (7.7%) returned PSD estimates which reached the 10% FAP threshold and 479 (47.9%) signals returned PSD estimates which reached the 50% FAP threshold. Based on our analysis using 1,000 signals, FAPs preforms better than expected for signals resampled to match the days for which an SO_2 emission rate is available at Mayon volcano.

21699356, 2022, 12, Downloaded from https://agupubs.onlinelibrary.wiley.com/doi/10.1029/2022JB025380 by Cochrane France, Wiley Online Library on [05/01/2023]. See the Terms and Conditions (https://onlinelibrary.wiley.com/terms-and-conditions) on Wiley Online Library for rules of use; OA articles are governed by the applicable Creative Commons License

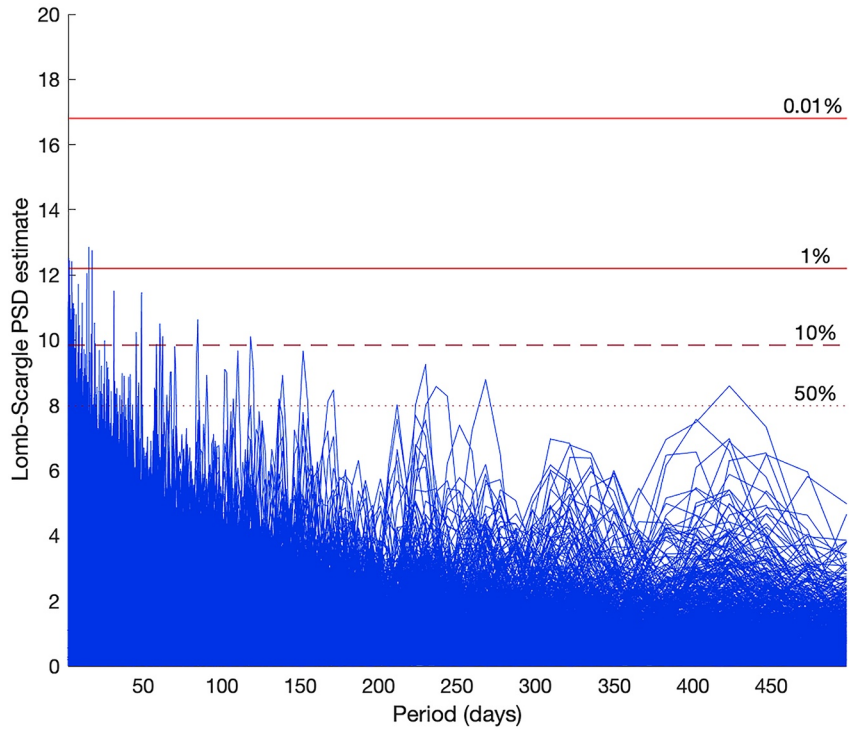

Figure B3. Lomb-Scargle PSD estimates of 1,000 signals comprised purely of Gaussian noise, rescaled, and resampled to match the magnitude of SO_2 emission rates reported and the days for which an SO_2 emission rate is available at Mayon volcano. FAPs are calculated with threshold values indicated for FAPs of 50% (8.0), 10% (9.9), 1% (12.2), and 0.01% (16.8).

Appendix C: Lomb-Scargle PSD Estimate of SO_2 Emission Rate for Volcanoes Included in the NOVAC Database

Figure C1displays the Lomb-Scargle PSD estimates of SO_2 emission rate for all volcanoes considered in this study.

Table C1.

21699356, 2022, 12, Downloaded from https://agupubs.onlinelibrary.wiley.com/doi/10.1029/2022JB025380 by Cochrane France, Wiley Online Library on [05/01/2023]. See the Terms and Conditions (https://onlinelibrary.wiley.com/terms-and-conditions) on Wiley Online Library for rules of use; OA articles are governed by the applicable Creative Commons License

10.1029/2022JB025380

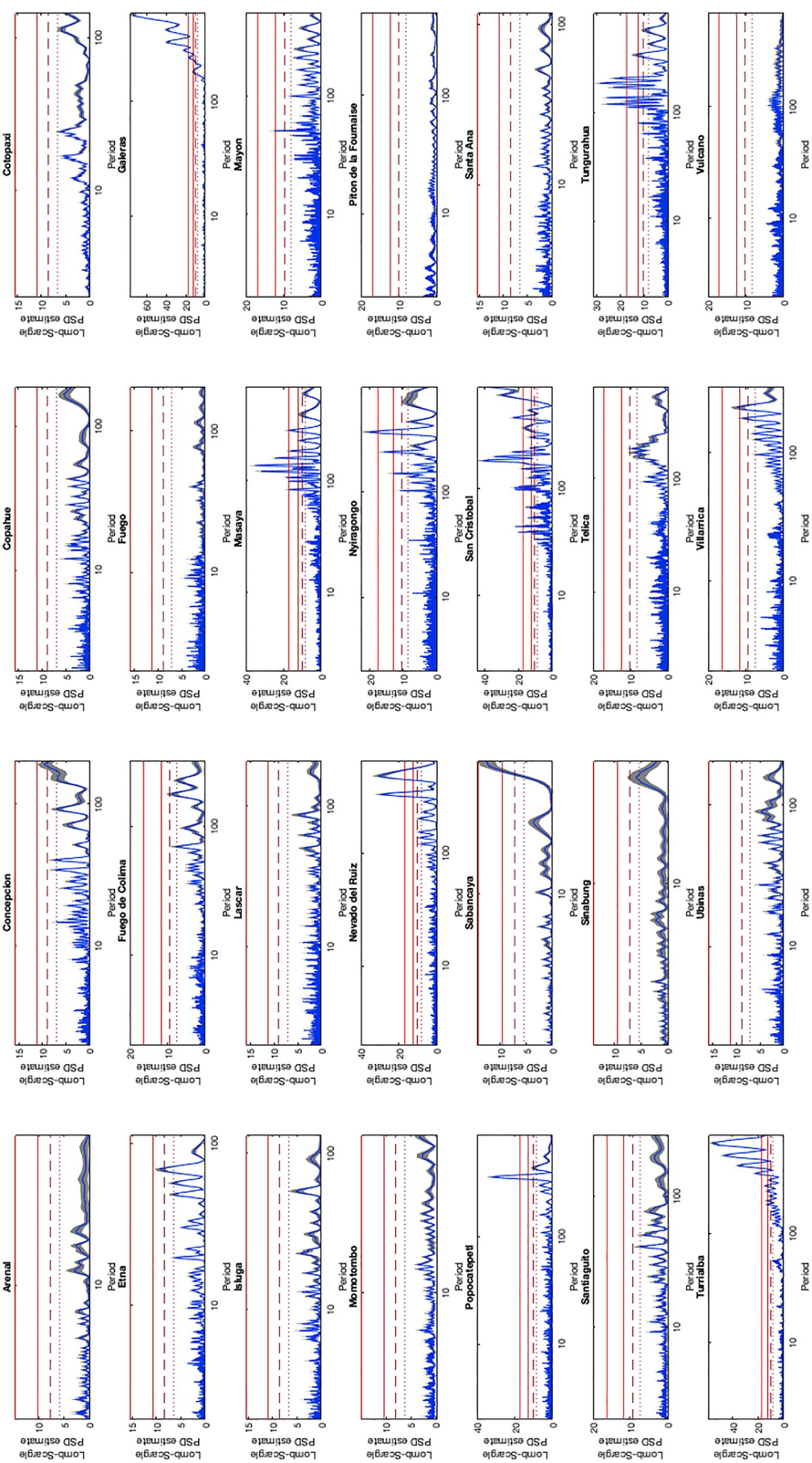

Figure C1. Lomb-Scargle Power Spectral Density (PSD) estimate of SO_2 emission rate for all volcanoes between the pseudo-Nyquist frequency and $N/4$, corresponding to 2 days and four-cycles per time series. Blue line corresponds to the median PSD estimate obtained by resampling the time series of SO_2 emission rate 1,000 times, between the minimum and maximum values on any given day. Standard deviation of the returned PSD estimates is shown in gray. Period is in days. Horizontal lines correspond to False Alarm Probability (FAP) of 50%, 10%, 1%, and 0.01%, see Table C1 for PSD threshold values associated with FAP at each volcano. Periodicities are considered statistically significant if the median PSD reaches the 50% FAP threshold, enabling rejection of the null hypothesis with at least 50% confidence.

21699356, 2022, 12, Downloaded from https://agupubs.onlinelibrary.wiley.com/doi/10.1029/2022JB025380 by Cochrane France, Wiley Online Library on [05/01/2023]. See the Terms and Conditions (https://onlinelibrary.wiley.com/terms-and-conditions) on Wiley Online Library for rules of use; OA articles are governed by the applicable Creative Commons License

21699356, 2022, 12, Downloaded from https://agupubs.onlinelibrary.wiley.com/doi/10.1029/2022JB025380 by Cochrane France, Wiley Online Library on [05/01/2023]. See the Terms and Conditions (https://onlinelibrary.wiley.com/terms-and-conditions) on Wiley Online Library for rules of use; OA articles are governed by the applicable Creative Commons License

Table C1
PSD Threshold Values Associated With FAP of SO_2 Emission Rates Shown Figures 8, C1, and D1

	FAP (%)			
Volcano	50	10	1	0.01
Arenal	5.9	7.8	10.1	14.7
Concepción	7.1	8.9	11.3	15.9
Copahue	7.0	8.9	11.2	15.8
Cotopaxi	6.7	8.6	11.0	15.6
Etna	6.5	8.4	10.7	15.3
Fuego de Colima	7.5	9.4	11.8	16.4
Fuego	7.1	9.0	11.3	15.9
Galeras	8.1	10.0	12.4	17.0
Isluga	6.6	8.5	10.9	15.5
Lascar	7.1	9.0	11.3	16.0
Masaya	8.3	10.2	12.5	17.1
Mayon	8.0	9.9	12.2	16.8
Momotombo	6.1	8.0	10.3	15.0
Nevado del Ruiz	8.2	10.1	12.5	17.1
Nyiragongo	8.6	10.5	12.9	17.5
Piton de la Fournaise	8.0	9.9	12.2	16.8
Popocatepetl	8.5	10.4	12.8	17.4
Sabancaya	5.5	7.4	9.7	14.3
San Cristobal	8.5	10.4	12.8	17.4
Santa Ana	6.6	8.4	10.8	15.4
Santiaguito	7.4	9.3	11.7	16.3
Sinabung	5.3	7.2	9.5	14.1
Telica	8.2	10.1	12.5	17.1
Tungurahua	8.5	10.3	12.7	17.3
Turrialba	8.4	10.3	12.7	17.3
Ubinas	7.1	9.0	11.3	15.9
Villarrica	7.5	9.4	11.8	16.4
Vulcano	8.3	10.2	12.6	17.2

Appendix D: Lomb-Scargle PSD Estimate of SO_2 Emission and PSD of Parameters Used to Determine SO_2 Emission Rate

D1. Reduction in PSD When Additional Periodicities Exist

Periodicities of 50, 57, and 70 days in the SO_2 emission rate at Etna volcano align with prominent peaks in the PSD estimate of plume speed, despite the latter not quite reaching the 50% FAP threshold (Figure 10). Our analysis of synthetic signals (Appendix B) highlights the possibility of missing genuine periodic trends when multiple periodicities exist (Figure 2). This may also be the case for the 137-day periodicity identified in the SO_2 emission rate at Tungurahua volcano as well as multiple peaks in the PSD estimate of SO_2 emission rate at San Cristobal (between 33 and 65 days). For plume speeds at both volcanoes, much larger PSD estimates are identified related to annual (355 days at Tungurahua) and interannual (185 days at Tungurahua, 183 days at San Cristobal) variability in-plume speed. We stress that in each case a distinct peak in the PSD estimate is evident (Figure D1).

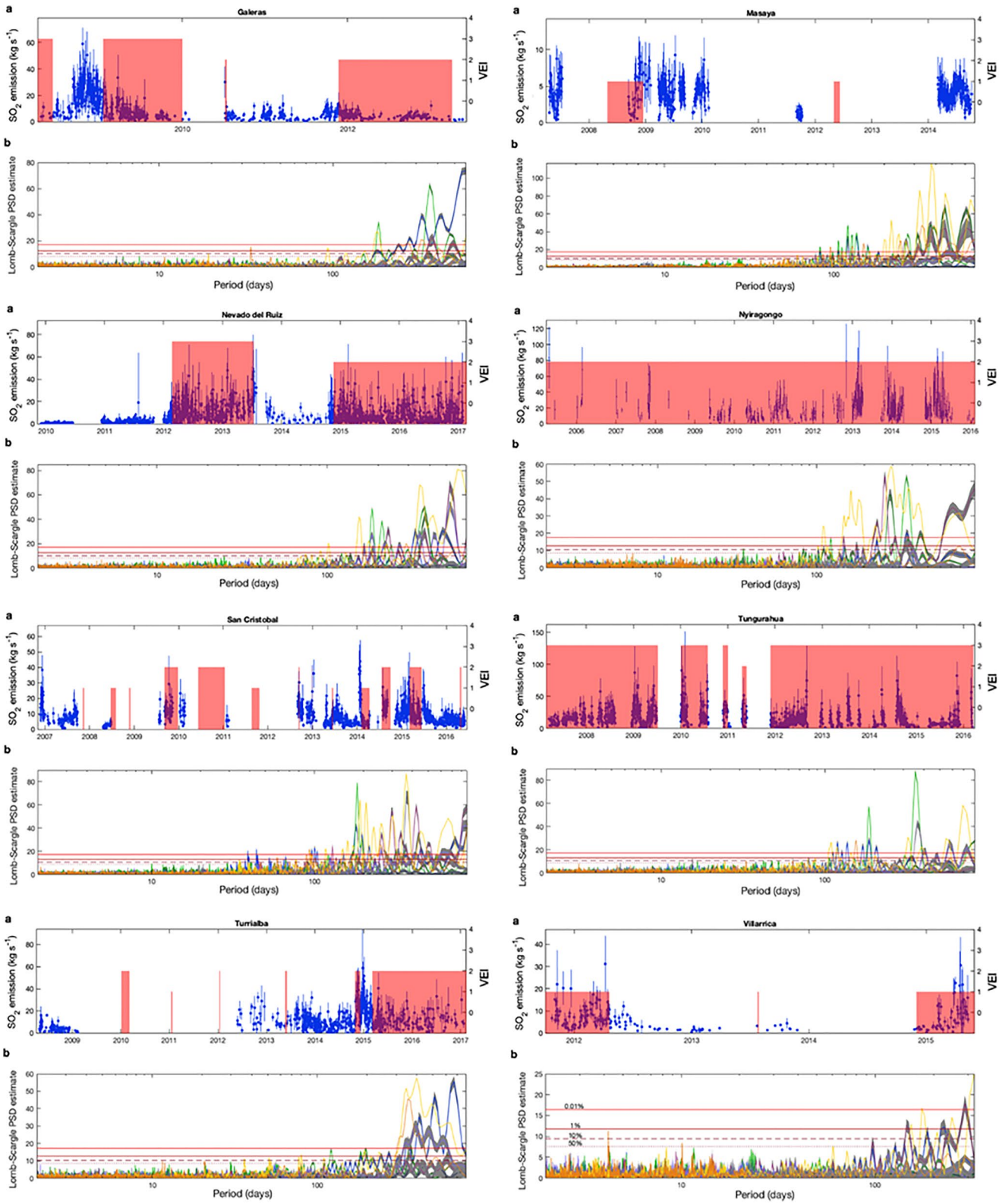

Figure D1.

21699356, 2022, 12, Downloaded from https://agupubs.onlinelibrary.wiley.com/doi/10.1029/2022JB025380 by Cochrane France, Wiley Online Library on [05/01/2023]. See the Terms and Conditions (https://onlinelibrary.wiley.com/terms-and-conditions) on Wiley Online Library for rules of use; OA articles are governed by the applicable Creative Commons License

21699356, 2022, 12, Downloaded from https://agupubs.onlinelibrary.wiley.com/doi/10.1029/2022JB025380 by Cochrane France, Wiley Online Library on [05/01/2023]. See the Terms and Conditions (https://onlinelibrary.wiley.com/terms-and-conditions) on Wiley Online Library for rules of use; OA articles are governed by the applicable Creative Commons License

D2. Offset in Returned Periodicities

Due to noise in the data, the highest peak returned in the PSD estimates often corresponds to an alias of the true period (VanderPlas, 2018). This may be the case where the PSD estimate of SO_2 emission rate and that of plume speed appear similar but identified periodicities appear offset. At Masaya, a 185-day periodicity in SO_2 emission rate may be related to the 180-day periodicity in-plume speed, particularly since all other periodicities identified in the SO_2 emission rate at Masaya are clearly associated with periodicities in-plume speed.

As highlighted by testing our approach with synthetic signals, it is possible for several median PSD estimates to cross the 50% FAP threshold but be associated to a single peak (Figure 2c). In the case of a small offset in the periodicities identified in SO_2 emission rate and plume speed, several PSD estimates will appear to represent a significant periodicity (i.e., cross 50% FAP threshold) but in fact be associated with a more prominent peak (with FAP < 50%).

D3. Strong Aliasing Across Multiple Parameters

For several volcanoes, peaks in the PSD estimates become indistinguishable from one another. Such aliasing pattern may be the result of several, indistinguishable periodic trends and highlights a limitation of FAPs (VanderPlas, 2018). This is apparent at both Turrialba and Galeras volcanoes. At Turrialba, broadly increasing PSD estimates of SO_2 emission rate (from 120 days) coincides with high PSD estimates for several parameters: total number of measurements, number of valid measurements and plume width. At Galeras, an aliasing pattern in PSD estimates of SO_2 emission rate overlaps with several periodicities in-plume speed (between 183 and 359 days).

Strong aliasing in the PSD estimate of SO_2 emission rate at Villarrica indicate periodic trend(s) between 127 and 227 days, which do not correspond to periodicities in-plume speed. However, a similar aliasing pattern is apparent in the PSD estimates of the distance to plume and number of measurements which may attribute observational bias to any periodic trends in the SO_2 emission rate.

A 327-day periodicity in SO_2 emission rate at Nevado del Ruiz is likely associated with a cluster of elevated PSD estimates (centered at ~360 days) across most parameters and likely related to the variability in weather during the year. A 239-day periodicity in SO_2 emission rate at Nyiragongo corresponds to periodicities in the number of measurements and distance to plume, both which may be related to the cluster of increased PSD estimates seen in most parameters between 235 and 450 days. Again, common observations between plume speed, plume direction, total number of measurements, and distance to plume are likely to reflect the annual and interannual variation in weather patterns. We note, however, strong aliasing in the PSD estimates of most parameters for both Nevado del Ruiz and Nyiragongo at periodicities >150 days.

Figure D1. Emission rate of SO_2 for volcanoes with periodicities in SO_2 emission unaccompanied by statistically significant periodicities in wind speed (see Figure 9). (a) Daily mean SO_2 emission rates are plotted as blue circles and error bars represent the corresponding standard deviation. Eruptive history is represented by red bars, using confirmed eruptions as defined in the Smithsonian's Global Volcanism Program database (Global Volcanism Project, 2013a). Where no eruption end date is listed, 10 days is used by default, unless it represents the most recent entry and therefore is considered an ongoing eruption. Emission rate data presented here are taken from the NOVAC Database; Galeras (Chacon et al., 2020a); Masaya (Saballos et al., 2020b); Nevado del Ruiz (Chacon et al., 2020b); Nyiragongo (Yalire et al., 2020); San Cristóbal (Saballos et al., 2020d); Tungurahua (Hidalgo et al., 2020b); Turrialba (Avard, Galle, & Arellano, 2020); and Villarrica (Velasquez et al., 2020b). (b) Lomb-Scargle Power Spectral Density (PSD) estimate of SO_2 emission and PSD of parameters used to determine SO_2 emission rate, at periods between the pseudo-Nyquist frequency and $N/4$. Median PSD estimates for each parameter are shown as single solid lines and corresponding standard deviation is shown in gray. Colors refer to the following parameters: SO_2 emission rate (blue), plume speed (light green), plume direction (dark green), distance to plume (magenta), plume width (lilac), cloud cover (gray), total measurements (yellow), and valid measurements (orange). Where the plume altitude has been determined by triangulation of two scans the Lomb-Scargle PSD estimate for plume altitude (navy) is shown. Horizontal lines correspond to False Alarm Probability (FAP) of 50%, 10%, 1%, and 0.01% (where some labels have been omitted for readability), see Table C1 for PSD threshold values associated with FAP at each volcano.

21699356, 2022, 12, Downloaded from https://agupubs.onlinelibrary.wiley.com/doi/10.1029/2022JB025380 by Cochrane France, Wiley Online Library on [05/01/2023]. See the Terms and Conditions (https://onlinelibrary.wiley.com/terms-and-conditions) on Wiley Online Library for rules of use; OA articles are governed by the applicable Creative Commons License

Data Availability Statement

All SO_2 emissions data and associated parameters used in this study are available via the NOVAC Database (licence CC BY 4.0) which may be found at https://novac.chalmers.se/ (NOVAC Project, 2020). Data from the NOVAC Database may be used providing all organizations and individuals are properly credited (https://novac.chalmers.se/datauseagreement). Zonal wind speed data used in this study are available through the European Centre for Medium-Range Weather Forecasts (ECMWF) at http://www.ecmwf.int/. © [2022] European Centre for Medium-Range Weather Forecasts (ECMWF, 2022). This data is published under a Creative Commons Attribution 4.0 International (CC BY 4.0) https://creativecommons.org/licenses/by/4.0/ and ECMWF does not accept any liability whatsoever for any error or omission in the data, their availability, or for any loss or damage arising from their use. We use MATLAB R2021a for all analysis which makes use of the "Plomb" function available via the Signal Processing Toolbox™. A copy of the code used in this manuscript is available at: https://zenodo.org/account/settings/github/repository/cbarrington22/Periodicities together with a user-friendly code which enables implementation of the method presented in this manuscript (https://doi.org/10.5281/zenodo.7304985).

Acknowledgments
We thank D. Tailpied for providing the ECMWF ERA-Interim data and acknowledge the ECMWF for the production of the reanalysis ERA5 data used in this research. We also wish to thank V. Burgos for the use of their volcano-database and for valuable discussions during the initial stages of this work as well as to M. Nguyen for their expert advice on time series analysis. We are especially grateful to all NOVAC members who have contributed to establishing the NOVAC Database which ultimately made this study possible. We are grateful to M. Poland for their suggestions and thank T. Lopez and one anonymous reviewer for their constructive reviews which helped improve the quality of this manuscript. This research was supported by the Earth Observatory of Singapore via its funding from the National Research Foundation Singapore and the Singapore Ministry of Education under the Research Centres of Excellence initiative. This work comprises EOS contribution number 464.

References

Aiuppa, A., Giudice, G., Liuzzo, M., Tamburello, G., Allard, P., Calabrese, S., et al. (2012). First volatile inventory for Gorely Volcano, Kamchatka: Volatile inventory for Gorley Volcano. *Geophysical Research Letters*, *39*, L06307. https://doi.org/10.1029/2012GL051177

Allard, P., Burton, M., Sawyer, G., & Bani, P. (2016). Degassing dynamics of basaltic lava lake at a top-ranking volatile emitter: Ambrym Volcano, Vanuatu arc. *Earth and Planetary Science Letters*, *448*, 69–80. https://doi.org/10.1016/j.epsl.2016.05.014

Arellano, S., Galle, B., Apaza, F., Avard, G., Barrington, C., Bobrowski, N., et al. (2021). Synoptic analysis of a decade of daily measurements of SO_2: Emission in the troposphere from volcanoes of the global ground-based Network for Observation of Volcanic and Atmospheric Change. *Earth System Science Data*, *13*(3), 1167–1188. https://doi.org/10.5194/essd-13-1167-2021

Aumento, F. (2002). Radon tides on an active volcanic island: Terceira, Azores. *Geofísica Internacional*, *41*, 499–505.

Avard, G., Arellano, S., De Moor, M., Duarte, E., Martinez, M., & Galle, B. (2020). SO_2 flux of TURRIALBA Volcano (Version 1) [Dataset]. NOVAC Database. https://doi.org/10.17196/NOVAC.TURRIALBA.001

Avard, G., Galle, B., & Arellano, S. (2020). SO_2 flux of ARENAL Volcano (Version 1) [Dataset]. NOVAC Database. https://doi.org/10.17196/NOVAC.ARENAL.001

Bani, P., & Lardy, M. (2007). Sulphur dioxide emission rates from Yasur Volcano, Vanuatu archipelago. *Geophysical Research Letters*, *34*, L20309. https://doi.org/10.1029/2007GL030411

Bao, J., Fotini, K. C., & Lundquist, K. A. (2018). Large-eddy simulation over complex terrain using an improved immersed boundary method in the weather research and forecasting model. *Monthly Weather Review*, *146*(9), 2781–2797. https://doi.org/10.1175/MWR-D-18-0067.1

Battaglia, A., Bitetto, M., Aiuppa, A., Rizzo, A. L., Chigna, G., Watson, I. M., et al. (2018). The magmatic gas signature of Pacaya Volcano, with implications for the volcanic CO_2 flux from Guatemala. *Geochemistry, Geophysics, Geosystems*, *19*, 667–692. https://doi.org/10.1002/2017GC007238

Bechmann, A., Sørensen, N. N., Berg, J., Mann, J., & Réthoré, P.-E. (2011). The Bolund experiment, Part II: Blind comparison of microscale flow models. *Boundary-Layer Meteorology*, *141*(2), 245–271. https://doi.org/10.1007/s10546-011-9637-x

Belousov, A., Voight, B., Belousova, M., & Petukhin, A. (2002). Pyroclastic surges and flows from the 8-10 May 1997 explosive eruption of Bezymianny Volcano, Kamchatka, Russia. *Bulletin of Volcanology*, *64*(7), 455–471. https://doi.org/10.1007/s00445-002-0222-5

Berberich, G. M., Berberich, M. B., Ellison, A. M., & Wöhler, C. (2019). First identification of periodic degassing rhythms in three mineral springs of the East Eifel Volcanic Field (EEVF, Germany). *Geosciences*, *9*(4), 189. https://doi.org/10.3390/geosciences9040189

Bernard, A., Escobar, C. D., Mazot, A., & Gutierrez, R. E. (2004). The acid volcanic lake of Santa Ana Volcano, El Salvador. In W. I. Rose, J. J. Bommer, D. L. López, M. J. Carr, & J. J. Major (Eds.), *Natural Hazards in El Salvador, Geological Society of America Special Papers* (Vol. 375, pp. 121–133). Geological Society of America. https://doi.org/10.1130/0-8137-2375-2.121

Bluth, G. J. S., Shannon, J. M., Watson, I. M., Prata, A. J., & Realmuto, V. J. (2007). Development of an ultra-violet digital camera for volcanic SO_2 imaging. *Journal of Volcanology and Geothermal Research*, *161*(1–2), 47–56. https://doi.org/10.1016/j.jvolgeores.2006.11.004

Borgia, A., & van Wyk de Vries, B. (2003). The volcano-tectonic evolution of Concepción, Nicaragua. *Bulletin of Volcanology*, *65*(4), 248–266. https://doi.org/10.1007/s00445-002-0256-8

Bornas, A., Arellano, S., Costa, F., Fernandez, D., Barrington, C., Redabulla, R., et al. (2020). SO_2 flux of MAYON Volcano (Version 1) [Dataset]. NOVAC Database. https://doi.org/10.17196/NOVAC.MAYON.001

Bottari, A., Caccamo, D., Montalto, A., Neri, G., & Privitera, E. (1992). Recent seismicity at Vulcano Island (Southern Italy) and adjacent regions: Time patterns and periodicities. In P. Gasparini, R. Scarpa, & K. Aki (Eds.), *Volcanic seismology. IAVCEI Proceedings in Volcanology* (Vol. 3, pp. 74–83). Springer. https://doi.org/10.1007/978-3-642-77008-1_6

Bouche, E., Vergniolle, S., Staudacher, T., Nercessian, A., Delmont, J.-C., Frogneux, M., et al. (2010). The role of large bubbles detected from acoustic measurements on the dynamics of Erta 'Ale lava lake (Ethiopia). *Earth and Planetary Science Letters*, *295*(1–2), 37–48. https://doi.org/10.1016/j.epsl.2010.03.020

Bredemeyer, S., & Hansteen, T. H. (2014). Synchronous degassing patterns of the neighbouring volcanoes Llaima and Villarrica in south-central Chile: The influence of tidal forces. *International Journal of Earth Science*, *103*(7), 1999–2012. https://doi.org/10.1007/s00531-014-1029-2

Bucarey, C., Arellano, S., Velasquez, G., & Galle, B. (2020a). SO_2 flux of ISLUGA Volcano (Version 1) [Dataset]. NOVAC Database. https://doi.org/10.17196/NOVAC.ISLUGA.001

Bucarey, C., Arellano, S., Velasquez, G., & Galle, B. (2020b). SO_2 flux of LASCAR Volcano (Version 1) [Dataset]. NOVAC Database. https://doi.org/10.17196/NOVAC.LASCAR.001

Campion, R., Delgado-Granados, H., Legrand, D., Taquet, N., Boulesteix, T., Pedraza-Espitía, S., & Lecocq, T. (2018). Breathing and coughing: The extraordinarily high degassing of Popocatépetl Volcano investigated with an SO_2 camera. *Frontiers of Earth Science*, *6*, 163. https://doi.org/10.3389/feart.2018.00163

Chacon, Z., Arellano, S., Burbano, V., Garzon, G., Laverde, C., & Galle, B. (2020a). SO_2 flux of GALERAS Volcano (Version 1) [Dataset]. NOVAC Database. https://doi.org/10.17196/NOVAC.GALERAS.001

Chacon, Z., Arellano, S., Garzon, G., Lopez, C., & Galle, B. (2020b). SO_2 flux of NEVADO.DEL.RUIZ Volcano (Version 1) [Dataset]. NOVAC Database. https://doi.org/10.17196/NOVAC.NEVADODELRUIZ.001

Chadwick, W. W., Jr., Geist, D. J., Jonsson, S., Poland, M., Johnson, D. J., & Meertens, C. M. (2006). A volcano bursting at the seams: Inflation, faulting, and eruption at Sierra Negra Volcano, Galapagos. *Geology*, *34*(12), 1025–1028. https://doi.org/10.1130/G22826A.1

Chigna, G., Arellano, S., Caceres, V., Sanchez, E., & Galle, B. (2020a). SO_2 flux of SANTIAGUITO Volcano (Version 1) [Dataset]. NOVAC Database. https://doi.org/10.17196/NOVAC.SANTIAGUITO.001

Chigna, G., Galle, B., & Arellano, S. (2020b). SO_2 flux of FUEGO.GUATEMALA Volcano (Version 1) [Dataset]. NOVAC Database. https://doi.org/10.17196/NOVAC.FUEGOGUATEMALA.001

Christopher, T., Edmonds, M., Taisne, B., Odbert, H., Costa, A., Hards, V., & Wadge, G. (2015). Periodic sulphur dioxide degassing from the Soufrière Hills Volcano related to deep magma supply. *Geological Society of London Special Publications*, *410*(1), 123–141. https://doi.org/10.1144/SP410.11

Cigolini, C., Poggi, P., Ripepe, M., Laiolo, M., Ciamberlini, C., Delle Donne, D., et al. (2009). Radon surveys and real-time monitoring at Stromboli Volcano: Influence of soil temperature, atmospheric pressure and tidal forces on ^{222}Rn degassing. *Journal of Volcanology and Geothermal Research*, *184*(3–4), 381–388. https://doi.org/10.1016/j.jvolgeores.2009.04.019

Conde, V., Bredemeyer, S., Duarte, E., Pacheco, J. F., Miranda, S., Galle, B., & Hansteen, T. H. (2014). SO_2 degassing from Turrialba Volcano linked to seismic signatures during the period 2008–2012. *International Journal of Earth Science*, *103*, 1983–1998. https://doi.org/10.1007/s00531-013-0958-5

Conde, V., Bredemeyer, S., Saballos, J. A., Galle, B., & Hansteen, T. H. (2016). Linking SO_2 emission rates and seismicity by continuous wavelet transform: Implications for volcanic surveillance at San Cristóbal Volcano, Nicaragua. *International Journal of Earth Science*, *105*(5), 1453–1465. https://doi.org/10.1007/s00531-015-1264-1

Connor, C. B., Stoiber, R. E., & Malinconico, L. L. (1988). Variation in sulfur dioxide emissions related to earth tides, Halemaumau Crater, Kilauea Volcano, Hawaii. *Journal of Geophysical Research*, *93*(B12), 14867–14871. https://doi.org/10.1029/JB093iB12p14867

Custodio, S. I. S., Fonseca, J. F. B. D., d'Oreye, N. F., Faria, B. V. E., & Bandomo, Z. (2003). Tidal modulation of seismic noise and volcanic tremor: Tidal modulation of seismic noise and volcanic tremor. *Geophysical Research Letters*, *30*(15), 1816. https://doi.org/10.1029/2003GL016991

Dee, D. P., Uppala, S. M., Simmons, A. J., Berrisford, P., Poli, P., Kobayashi, S., et al. (2011). The ERA-Interim reanalysis: Configuration and performance of the data assimilation system. *Quarterly Journal of the Royal Meteorological Society*, *137*(656), 553–597. https://doi.org/10.1002/qj.828

Delgado, H., Arellano, S., Rivera, C., Fickel, M., Alvarez, J., & Galle, B. (2020a). SO_2 flux of FUEGO.DE.COLIMA Volcano (Version 1) [Dataset]. NOVAC Database. https://doi.org/10.17196/NOVAC.FUEGODECOLIMA.001

Delgado, H., Arellano, S., Rivera, C., Fickel, M., Alvarez, J., & Galle, B. (2020b). SO_2 flux of POPOCATEPETL Volcano (Version 1) [Dataset]. NOVAC Database. https://doi.org/10.17196/NOVAC.POPOCATEPETL.001

DiMuro, A., Arellano, S., Kowalski, P., Staudacher, T., Garofalo, K., & Galle, B. (2020). SO_2 flux of PITON.DE.LA.FOURNAISE Volcano (Version 1) [Dataset]. NOVAC Database. https://doi.org/10.17196/NOVAC.PITONDELAFOURNAISE.001

Dinger, F., Bobrowski, N., Warnach, S., Bredemeyer, S., Hidalgo, S., Arellano, S., et al. (2018). Periodicity in the BrO/SO_2 molar ratios in the volcanic gas plume of Cotopaxi and its correlation with the Earth tides during the eruption in 2015. *Solid Earth*, *9*, 247–266. https://doi.org/10.5194/se-9-247-2018

Dinger, F., Bredemeyer, S., Arellano, S., Bobrowski, N., Platt, U., & Wagner, T. (2019). On the link between Earth tides and volcanic degassing. *Solid Earth*, *10*, 725–741. https://doi.org/10.5194/se-10-725-2019

Dinger, F., Kleinbek, T., Dörner, S., Bobrowski, N., Platt, U., Wagner, T., et al. (2021). SO_2 and BrO emissions of Masaya Volcano from 2014–2020. *Atmospheric Chemistry and Physics*, *21*(12), 9367–9404. https://doi.org/10.5194/acp-21-9367-2021

Ebisuzaki, T., Miyahara, H., Kataoka, R., Sato, T., & Ishimine, Y. (2011). Explosive volcanic eruptions triggered by cosmic rays: Volcano as a bubble chamber. *Gondwana Research*, *19*(4), 1054–1061. https://doi.org/10.1016/j.gr.2010.11.004

ECMWF. (2022). European Centre for Medium-Range Weather Forecasts [Dataset]. Retrieved from https://www.ecmwf.int/

Edmonds, M., Oppenheimer, C., Pyle, D. M., Herd, R. A., & Thompson, G. (2003). SO_2 emissions from Soufrière Hills Volcano and their relationship to conduit permeability, hydrothermal interaction and degassing regime. *Journal of Volcanology and Geothermal Research*, *124*(1–2), 23–43. https://doi.org/10.1016/S0377-0273(03)00041-6

Fadeli, A., Rydelek, P., Emter, D., & Ziirn, W. (1991). On volcanic shocks at Merapi and tidal triggering. In R. Schick, & R. Mugiano (Eds.), *Volcanic Tremor and Magma Flow, Scientific Series of the International Bureau* (Vol. 4, pp. 165–181). Forschungszentrum Jülich.

Favalli, M., Mazzarini, F., Pareschi, M. T., & Boschi, E. (2004). Role of local wind circulation in plume monitoring at Mt. Etna volcano (Sicily): Insights from a mesoscale numerical model. *Geophysical Research Letters*, *31*, L09105. https://doi.org/10.1029/2003GL019281

Filson, J., Simkin, T., & Leu, L. (1973). Seismicity of a caldera collapse: Galapagos Islands 1968. *Journal of Geophysical Research*, *78*(35), 8591–8622. https://doi.org/10.1029/JB078i035p08591

Flower, V. J. B., & Carn, S. A. (2015). Characterising volcanic cycles at Soufriere Hills Volcano, Montserrat: Time series analysis of multi-parameter satellite data. *Journal of Volcanology and Geothermal Research*, *304*, 82–93. https://doi.org/10.1016/j.jvolgeores.2015.07.035

Galle, B., Johansson, M., Rivera, C., Zhang, Y., Kihlman, M., Kern, C., et al. (2010). Network for Observation of Volcanic and Atmospheric Change (NOVAC)—A global network for volcanic gas monitoring: Network layout and instrument description. *Journal of Geophysical Research*, *115*, D05304. https://doi.org/10.1029/2009JD011823

Galle, B., Oppenheimer, C., Geyer, A., McGonigle, A. J. S., Edmonds, M., & Horrocks, L. (2002). A miniaturised ultraviolet spectrometer for remote sensing of SO_2 fluxes: A new tool for volcano surveillance. *Journal of Volcanology and Geothermal Research*, *119*(1–4), 241–254. https://doi.org/10.1016/S0377-0273(02)00356-6

Girona, T., Costa, F., Taisne, B., Aggangan, B., & Ildefonso, S. (2015). Fractal degassing from Erebus and Mayon volcanoes revealed by a new method to monitor H_2O emission cycles. *Journal of Geophysical Research: Solid Earth*, *120*, 2988–3002. https://doi.org/10.1002/2014JB011797

Girona, T., Huber, C., & Caudron, C. (2018). Sensitivity to lunar cycles prior to the 2007 eruption of Ruapehu Volcano. *Scientific Reports*, *8*(1), 1476. https://doi.org/10.1038/s41598-018-19307-z

Global Volcanism Project. (2013b). *Mayon (273030), Volcanoes of the World (Version 4.11.0)* [Dataset]. In E. Venzke (Ed.), *Smithsonian Institution*. Retrieved from https://volcano.si.edu/volcano.cfm?vn=273030

Global Volcanism Project. (2013a). *Volcanoes of the World (Version 4.11.0)* [Dataset]. In E. Venzke (Ed.), *Smithsonian Institution*. https://doi.org/10.5479/si.GVP.VOTW4-2013

21699356, 2022, 12, Downloaded from https://agupubs.onlinelibrary.wiley.com/doi/10.1029/2022JB025380 by Cochrane France, Wiley Online Library on [05/01/2023]. See the Terms and Conditions (https://onlinelibrary.wiley.com/terms-and-conditions) on Wiley Online Library for rules of use; OA articles are governed by the applicable Creative Commons License

Granieri, D., Chiodini, G., Marzocchi, W., & Avino, R. (2003). Continuous monitoring of CO_2 soil diffuse degassing at Phlegraean Fields (Italy): Influence of environmental and volcanic parameters. *Earth and Planetary Science Letters*, *212*(1–2), 167–179. https://doi.org/10.1016/S0012-821X(03)00232-2

Helbig, N., Mott, R., van Herwijnen, A., & Jonas, T. (2017). Parameterizing surface wind speed over complex topography. *Journal of Geophysical Research: Atmospheres*, *122*, 651–667. https://doi.org/10.1002/2016JD025593

Hidalgo, S., Arellano, S., Vasconez, F., Arrais, S., Bourquin, J., Cordova, J., & Galle, B. (2020a). SO_2 flux of COTOPAXI Volcano (Version 1) [Dataset]. NOVAC Database. https://doi.org/10.17196/NOVAC.COTOPAXI.001

Hidalgo, S., Arellano, S., Vasconez, F., Arrais, S., Bourquin, J., & Galle, B. (2020b). SO_2 flux of TUNGURAHUA Volcano (Version 1) [Dataset]. NOVAC Database. https://doi.org/10.17196/NOVAC.TUNGURAHUA.001

Hidalgo, S., Battaglia, J., Arellano, S., Sierra, D., Bernard, B., Parra, R., et al. (2018). Evolution of the 2015 Cotopaxi eruption revealed by combined geochemical and seismic observations. *Geochemistry, Geophysics, Geosystems*, *19*, 2087–2108. https://doi.org/10.1029/2018GC007514

Holland, A. S. P., Watson, I. M., Phillips, J. C., Caricchi, L., & Dalton, M. P. (2011). Degassing processes during lava dome growth: Insights from Santiaguito lava dome, Guatemala. *Journal of Volcanology and Geothermal Research*, *202*(1–2), 153–166. https://doi.org/10.1016/j.jvolgeores.2011.02.004

Jaggar, T. A., Finch, R. H., & Emerson, O. H. (1924). The lava tide seasonal tilt and the volcanic cycle. *Monthly Weather Review*, *52*(3), 142–145. https://doi.org/10.1175/1520-0493(1924)52<142:tltsta>2.0.co;2

Jentzsch, G., Haase, O., Kroner, C., & Winter, U. (2001). Mayon Volcano, Philippines: Some insights into stress balance. *Journal of Volcanology and Geothermal Research*, *109*(1–3), 205–217. https://doi.org/10.1016/S0377-0273(00)00312-7

Johansson, M., Galle, B., Zhang, Y., Rivera, C., Chen, D., & Wyser, K. (2009). The dual-beam mini-DOAS technique—Measurements of volcanic gas emission, plume height and plume speed with a single instrument. *Bulletin of Volcanology*, *71*(7), 747–751. https://doi.org/10.1007/s00445-008-0260-8

Johnson, M. J. S., Mauk, F. J., & Whyman, A. J. (1972). Earth tides and the triggering of eruptions from Mt Stromboli, Italy. *Nature*, *239*(5370), 267–269. https://doi.org/10.1038/239267a0

Kasahara, J., Nakao, S., & Koketsu, K. (2001). Tidal influence on the 2000 Miyake Jima eruption and its implications for hydrothermal activity and volcanism. *Proceedings of the Japan Academy Series B*, *77*(6), 98–103. https://doi.org/10.2183/pjab.77.98

Kasbani, K., Arellano, S., Gunawan, H., Haerani, N., Kunrat, S., Kern, C., & Galle, B. (2020). SO_2 flux of SINABUNG Volcano (Version 1) [Dataset]. NOVAC Database. https://doi.org/10.17196/NOVAC.SINABUNG.001

Kern, C., Deutschmann, T., Vogel, L., Wöhrbach, M., Wagner, T., & Platt, U. (2010). Radiative transfer corrections for accurate spectroscopic measurements of volcanic gas emissions. *Bulletin of Volcanology*, *72*(2), 233–247. https://doi.org/10.1007/s00445-009-0313-7

Laiolo, M., Ranaldi, M., Tarchini, L., Carapezza, M. L., Coppola, D., Ricci, T., & Cigolini, C. (2016). The effects of environmental parameters on diffuse degassing at Stromboli Volcano: Insights from joint monitoring of soil CO_2 flux and radon activity. *Journal of Volcanology and Geothermal Research*, *315*, 65–78. https://doi.org/10.1016/j.jvolgeores.2016.02.004

Lamb, O. D., Varley, N. R., Mather, T. A., Pyle, D. M., Smith, P. J., & Liu, E. J. (2014). Multiple timescales of cyclical behaviour observed at two dome-forming eruptions. *Journal of Volcanology and Geothermal Research*, *284*, 106–121. https://doi.org/10.1016/j.jvolgeores.2014.07.013

Lewicki, J. L., Hilley, G. E., Tosha, T., Aoyagi, R., Yamamoto, K., & Benson, S. M. (2007). Dynamic coupling of volcanic CO_2 flow and wind at the Horseshoe Lake tree kill, Mammoth Mountain, California. *Geophysical Research Letters*, *34*, L03401. https://doi.org/10.1029/2006GL028848

Lomb, N. R. (1976). Least-squares frequency analysis of unequally spaced data. *Astrophysics and Space Science*, *39*(2), 447–462. https://doi.org/10.1007/BF00648343

Lopez, T., Carn, S., Werner, C., Fee, D., Kelly, P., Doukas, M., et al. (2013). Evaluation of Redoubt Volcano's sulfur dioxide emissions by the Ozone Monitoring Instrument. *Journal of Volcanology and Geothermal Research*, *259*, 290–307. https://doi.org/10.1016/j.jvolgeores.2012.03.002

Lübcke, P., Lampel, J., Arellano, S., Bobrowski, N., Dinger, F., Galle, B., et al. (2016). Retrieval of absolute SO_2 column amounts from scattered-light spectra: Implications for the evaluation of data from automated DOAS networks. *Atmospheric Measurement Techniques*, *9*(12), 5677–5698. https://doi.org/10.5194/amt-9-5677-2016

Luhr, J. F., & Carmichael, I. S. E. (1980). The Colima Volcanic complex, Mexico: I. Post-caldera andesites from Volcán Colima. *Contributions to Mineralogy and Petrology*, *71*(4), 343–372. https://doi.org/10.1007/BF00374707

Luo, H., Ge, F., Yang, K., Zhu, S., Peng, T., Cai, W., et al. (2019). Assessment of ECMWF reanalysis data in complex terrain: Can the CERA-20C and ERA-Interim data sets replicate the variation in surface air temperatures over Sichuan, China? *International Journal of Climatology*, *39*(15), 5619–5634. https://doi.org/10.1002/joc.6175

Lyons, J. J., Waite, G. P., Rose, W. I., & Chigna, G. (2010). Patterns in open vent, strombolian behavior at Fuego Volcano, Guatemala, 2005–2007. *Bulletin of Volcanology*, *72*, 1. https://doi.org/10.1007/s00445-009-0305-7

Machado, F. (1967). Activity of the Atlantic volcanoes, 1947–1965. *Bulletin of Volcanology*, *30*(1), 29–34. https://doi.org/10.1007/BF02597652

Madden, R. A., & Julian, P. R. (1971). Detection of a 40–50 day oscillation in the zonal wind in the tropical Pacific. *Journal of the Atmospheric Sciences*, *28*(5), 702–708. https://doi.org/10.1175/1520-0469(1971)028<0702:doadoi>2.0.co;2

Madden, R. A., & Julian, P. R. (1972). Description of global-scale circulation cells in the tropics with a 40–50 day period. *Journal of the Atmospheric Sciences*, *29*(6), 1109–1123. https://doi.org/10.1175/1520-0469(1972)029<1109:dogscc>2.0.co;2

Madden, R. A., & Julian, P. R. (1994). Observations of the 40–50-day tropical oscillation—A review. *Monthly Weather Review*, *122*(5), 814–837. https://doi.org/10.1175/1520-0493(1994)122<0814:ootdto>2.0.co;2

Martin, E. R., & Schumacher, C. (2011). Modulation of Caribbean precipitation by the Madden-Julian Oscillation. *Journal of Climate*, *24*(3), 813–824. https://doi.org/10.1175/2010JCLI3773.1

Martinelli, B. (1990). Analysis of seismic patterns observed at Nevado del Ruiz Volcano, Colombia during August-September 1985. *Journal of Volcanology and Geothermal Research*, *41*(1–4), 297–314. https://doi.org/10.1016/0377-0273(90)90093-U

Masias, P., Arellano, S., Apaza, F., & Galle, B. (2020a). SO_2 flux of UBINAS Volcano, from the NOVAC data-base. https://doi.org/10.17196/NOVAC.UBINAS.001

Masias, P., Arellano, S., Apaza, F., Kern, C., & Galle, B. (2020b). SO_2 flux of SABANCAYA Volcano (Version 1) [Dataset]. NOVAC Database. https://doi.org/10.17196/NOVAC.SABANCAYA.001

MathWorks. (2021). *MATLAB*. The MathWorks Inc.

Matsumoto, J., Olaguera, L. M. P., Nguyen-Le, D., Kubota, H., & Villafuerte, M. Q., II. (2020). Climatological seasonal changes of wind and rainfall in the Philippines. *International Journal of Climatology*, *40*(11), 4843–4857. https://doi.org/10.1002/joc.6492

Matthews, S. J., Gardeweg, M. C., & Sparks, R. S. J. (1997). The 1984 to 1996 cyclic activity of Lascar Volcano, northern Chile: Cycles of dome growth, dome subsidence, degassing and explosive eruptions. *Bulletin of Volcanology*, *59*(1), 72–82. https://doi.org/10.1007/s004450050176

Mauk, F. J., & Kienle, J. (1973). Microearthquakes at St. Augustine Volcano, Alaska, triggered by earth tides. *Science*, *182*(4110), 386–389. https://doi.org/10.1126/science.182.4110.386

21699356, 2022, 12, Downloaded from https://agupubs.onlinelibrary.wiley.com/doi/10.1029/2022JB025380 by Cochrane France, Wiley Online Library on [05/01/2023]. See the Terms and Conditions (https://onlinelibrary.wiley.com/terms-and-conditions) on Wiley Online Library for rules of use; OA articles are governed by the applicable Creative Commons License

McNutt, S. R., & Beavan, R. J. (1981). Volcanic earthquakes at Pavlof Volcano correlated with the solid earth tide. *Nature*, *294*(5842), 615–618. https://doi.org/10.1038/294615a0

McNutt, S. R., & Beavan, R. J. (1984). Patterns of earthquakes and the effect of solid earth and ocean load tides at Mount St. Helens prior to the May 18, 1980, eruption. *Journal of Geophysical Research*, *89*(B5), 3075–3086. https://doi.org/10.1029/JB089iB05p03075

Melson, W. G., & Saenz, R. (1973). Volume, energy and cyclicity of eruptions of Arenal Volcano, Costa Rica. *Bulletin of Volcanology*, *37*(3), 416–437. https://doi.org/10.1007/BF02597639

Mengistu Tsidu, G., Blumenstock, T., & Hase, F. (2015). Observations of precipitable water vapour over complex topography of Ethiopia from ground-based GPS, FTIR, radiosonde and ERA-Interim reanalysis. *Atmospheric Measurement Techniques*, *8*, 3277–3295. https://doi.org/10.5194/amt-8-3277-2015

Michael, M. O., & Christoffel, D. A. (1975). Triggering of eruptions of Mt Ngauruhoe by fortnightly earth tide maxima, January 1972–June 1974. *New Zealand Journal of Geology and Geophysics*, *18*(2), 273–277. https://doi.org/10.1080/00288306.1975.10418198

Michaut, C., Ricard, Y., Bercovici, D., & Sparks, R. S. J. (2013). Eruption cyclicity at silicic volcanoes potentially caused by magmatic gas waves. *Nature Geoscience*, *6*(10), 856–860. https://doi.org/10.1038/ngeo1928

Millan, M. M. (1980). Remote sensing of air pollutants: A study of some atmospheric scattering effects. *Atmospheric Environment*, *14*(11), 1241–1253. https://doi.org/10.1016/0004-6981(80)90226-7

Montalvo, F., Arellano, S., Conde, V., Escobar, D., Barahona, F., Olmos, R., & Galle, B. (2020). SO_2 flux of SANTA.ANA Volcano (Version 1) [Dataset]. NOVAC Database. https://doi.org/10.17196/novac.santaana.001

Mori, J., White, R. A., Harlow, D. H., Okubo, P., Power, J. A., Hoblitt, R. P., et al. (1996). Volcanic earthquakes following the 1991 climactic eruption of mount Pinatubo: Strong seismicity during a waning eruption. In C. G.Newhall & R. S. Punongbayan (Eds.), *Fire and mud: Eruptions and Lahars of Mount Pinatubo* (pp. 339–350).Philippine Institute of Volcanology and Seismology Quezon City University of Washington Press Seattle and London.

Moussallam, Y., Tamburello, G., Peters, N., Apaza, F., Schipper, C. I., Curtis, A., et al. (2017). Volcanic gas emissions and degassing dynamics at Ubinas and Sabancaya volcanoes: Implications for the volatile budget of the central volcanic zone. *Journal of Volcanology and Geothermal Research*, *343*, 181–191. https://doi.org/10.1016/j.jvolgeores.2017.06.027

Muñoz, E., Busalacchi, A. J., Nigam, S., & Ruiz-Barradas, A. (2008). Winter and summer structure of the Caribbean low-level jet. *Journal of Climate*, *21*(6), 1260–1276. https://doi.org/10.1175/2007JCLI1855.1

Nadeau, P. A., Palma, J. L., & Waite, G. P. (2011). Linking volcanic tremor, degassing, and eruption dynamics via SO_2 imaging. *Geophysical Research Letters*, *38*, L01304. https://doi.org/10.1029/2010GL045820

Nadeau, P. A., & Williams-Jones, G. (2009). Apparent downwind depletion of volcanic SO_2 flux—Lessons from Masaya Volcano, Nicaragua. *Bulletin of Volcanology*, *71*(4), 389–400. https://doi.org/10.1007/s00445-008-0251-9

Nakada, S., Shimizu, H., & Ohta, K. (1999). Overview of the 1990–1995 eruption at Unzen Volcano. *Journal of Volcanology and Geothermal Research*, *89*(1–4), 1–22. https://doi.org/10.1016/S0377-0273(98)00118-8

Nakada, S., Zaennudin, A., Yoshimoto, M., Maeno, F., Suzuki, Y., Hokanishi, N., et al. (2019). Growth process of the lava dome/flow complex at Sinabung Volcano during 2013–2016. *Journal of Volcanology and Geothermal Research*, *382*, 120–136. https://doi.org/10.1016/j.jvolgeores.2017.06.012

Neuberg, J. (2000). External modulation of volcanic activity. *Geophysical Journal International*, *142*(1), 232–240. https://doi.org/10.1046/j.1365-246x.2000.00161.x

Neuberg, J. W., Collinson, A. S. D., Mothes, P. A., Ruiz, M. C., & Aguaiza, S. (2018). Understanding cyclic seismicity and ground deformation patterns at volcanoes: Intriguing lessons from Tungurahua Volcano, Ecuador. *Earth and Planetary Science Letters*, *482*, 193–200. https://doi.org/10.1016/j.epsl.2017.10.050

Nicholson, E. J., Mather, T. A., Pyle, D. M., Odbert, H. M., & Christopher, T. (2013). Cyclical patterns in volcanic degassing revealed by SO_2 flux timeseries analysis: An application to Soufrière Hills Volcano, Montserrat. *Earth and Planetary Science Letters*, *375*, 209–221. https://doi.org/10.1016/j.epsl.2013.05.032

NOVAC Project. (2020). NOVAC Database. Website. Retrieved from https://novac.chalmers.se/

NOVAC Project. (2022). Network for Observation of Volcanic and Atmospheric Change. Website. Retrieved from https://novac-community.org/

Nyquist, H. (1928). Certain topics in telegraph transmission theory. *Transactions on Electrical and Electronic Engineering*, *47*(2), 617–644. https://doi.org/10.1109/T-AIEE.1928.5055024

Oke, T. R. (1987). *Boundary layer climates* (2nd ed.). Routledge.

Palmieri, L. (1873). *The eruption of Vesuvius in 1872 (R. Mallet, Trans.)*. Asher & Company.

Peltier, A., Famin, V., Bachèlery, P., Cayol, V., Fukushima, Y., & Staudacher, T. (2008). Cyclic magma storages and transfers at Piton de La Fournaise Volcano (La Réunion hotspot) inferred from deformation and geochemical data. *Earth and Planetary Science Letters*, *270*(3–4), 180–188. https://doi.org/10.1016/j.epsl.2008.02.042

Pering, T. D., Ilanko, T., & Liu, E. J. (2019). Periodicity in volcanic gas plumes: A review and analysis. *Geosciences*, *9*, 394. https://doi.org/10.3390/geosciences9090394

Posada-Marín, J. A., Rendón, A. M., Salazar, J. F., Mejía, J. F., & Villegas, J. C. (2019). WRF downscaling improves ERA-Interim representation of precipitation around a tropical Andean valley during El Niño: Implications for GCM-scale simulation of precipitation over complex terrain. *Climate Dynamics*, *52*(5–6), 3609–3629. https://doi.org/10.1007/s00382-018-4403-0

Powers, J. G., Klemp, J. B., Skamarock, W. C., Davis, C. A., Dudhia, J., Gill, D. O., et al. (2017). The Weather Research and Forecasting model: Overview, system efforts, and future directions. *Bulletin of the American Meteorological Society*, *98*(8), 1717–1737. https://doi.org/10.1175/BAMS-D-15-00308.1

Ramos, E. G., de Torres, C. B., & Calderon, A. C. (1985). Earth tide influence on the recent activities of Mayon Volcano. *Philippine Journal of Volcanology*, *2*, 172–190.

Renault, L., & Marchesiello, P. (2022). Ocean tides can drag the atmosphere and cause tidal winds over broad continental shelves. *Communications Earth & Environment*, *3*(1), 70. https://doi.org/10.1038/s43247-022-00403-y

Ripepe, M., Harris, A. J. L., & Carniel, R. (2002). Thermal, seismic and infrasonic evidences of variable degassing rates at Stromboli Volcano. *Journal of Volcanology and Geothermal Research*, *118*(3–4), 285–297. https://doi.org/10.1016/S0377-0273(02)00298-6

Rose, W. I. (1987). Volcanic activity at Santiaguito volcano, 1976–1984. In J. H. Fink (Ed.), *The emplacement of silicic domes and lava flows, Geological Society of America Special Papers* (Vol. 212, pp. 17–27). Geological Society of America. https://doi.org/10.1130/SPE212-P17

Rotach, M. W., Gohm, A., Lang, M. N., Leukauf, D., Stiperski, I., & Wagner, J. S. (2015). On the vertical exchange of heat, mass, and momentum over complex mountainous terrain. *Frontiers of Earth Science*, *3*, 76. https://doi.org/10.3389/feart.2015.00076

Rymer, H. (2005). Magma plumbing processes for persistent activity at Poás Volcano, Costa Rica. *Geophysical Research Letters*, *32*, L08307. https://doi.org/10.1029/2004GL022284

21699356, 2022, 12, Downloaded from https://agupubs.onlinelibrary.wiley.com/doi/10.1029/2022JB025380 by Cochrane France, Wiley Online Library on [05/01/2023]. See the Terms and Conditions (https://onlinelibrary.wiley.com/terms-and-conditions) on Wiley Online Library for rules of use; OA articles are governed by the applicable Creative Commons License

Saballos, A., Arellano, S., Mendoza, E., Alvarez, J., Munoz, A., & Galle, B. (2020a). SO_2 flux of CONCEPCION Volcano (Version 1) [Dataset]. NOVAC Database. https://doi.org/10.17196/NOVAC.CONCEPCION.001

Saballos, A., Arellano, S., Mendoza, E., Alvarez, J., Munoz, A., & Galle, B. (2020b). SO_2 flux of MASAYA Volcano (Version 1) [Dataset]. NOVAC Database. https://doi.org/10.17196/NOVAC.MASAYA.001

Saballos, A., Arellano, S., Mendoza, E., Alvarez, J., Muñoz, A., & Galle, B. (2020c). SO_2 flux of MOMOTOMBO Volcano (Version 1) [Dataset]. NOVAC Database. https://doi:10.17196/NOVAC.MOMOTOMBO.001

Saballos, A., Arellano, S., Mendoza, E., Alvarez, J., Munoz, A., & Galle, B. (2020d). SO_2 flux of MASAYA Volcano (Version 1) [Dataset]. NOVAC Database. https://doi.org/10.17196/NOVAC.SANCRISTOBAL.001

Saballos, A., Arellano, S., Mendoza, E., Alvarez, J., Munoz, A., & Galle, B. (2020e). SO_2 flux of TELICA volcano (Version 1) [Dataset]. NOVAC Database. https://doi.org/10.17196/NOVAC.TELICA.001

Salazar, J. M. L., Hernandez, P. A., Perez, N. M., Olmos, R., Barahona, F., Cartagena, R., et al. (2004). Spatial and temporal variations of diffuse CO_2 degassing at the Santa Ana-Izalco-Coatepeque volcanic complex, El Salvador, Central America. In W. I. Rose, J. J. Bommer, D. L. López, M. J. Carr, & J. J. Major (Eds.), *Natural Hazards in El Salvador, Geological Society of America Special Papers* (Vol. 375, pp. 135–146). Geological Society of America. https://doi.org/10.1130/0-8137-2375-2.135

Salerno, G., Arellano, S., Burton, M., & Galle, B. (2020). SO_2 flux of ETNA Volcano (Version 1) [Dataset]. NOVAC Database. https://doi.org/10.17196/NOVAC.ETNA.001

Scargle, J. D. (1982). Studies in astronomical time series analysis. II—Statistical aspects of spectral analysis of unevenly spaced data. *The Astrophysical Journal*, *263*, 835. https://doi.org/10.1086/160554

Sottili, G., Martino, S., Palladino, D. M., Paciello, A., & Bozzano, F. (2007). Effects of tidal stresses on volcanic activity at Mount Etna, Italy. *Geophysical Research Letters*, *34*, L01311. https://doi.org/10.1029/2006GL028190

Stoiber, R. E., Williams, S. N., & Huebert, B. J. (1986). Sulfur and halogen gases at Masaya Caldera Complex, Nicaragua: Total flux and variations with time. *Journal of Geophysical Research*, *91*(B12), 12215–12231. https://doi.org/10.1029/JB091iB12p12215

Sweeney, D., Kyle, P. R., & Oppenheimer, C. (2008). Sulfur dioxide emissions and degassing behavior of Erebus Volcano, Antarctica. *Journal of Volcanology and Geothermal Research*, *177*(3), 725–733. https://doi.org/10.1016/j.jvolgeores.2008.01.024

Tamburello, G., Aiuppa, A., McGonigle, A. J. S., Allard, P., Cannata, A., Giudice, G., et al. (2013). Periodic volcanic degassing behavior: The Mount Etna example. *Geophysical Research Letters*, *40*, 4818–4822. https://doi.org/10.1002/grl.50924

Telling, J., Flower, V. J. B., & Carn, S. A. (2015). A multi-sensor satellite assessment of SO_2 emissions from the 2012–13 eruption of Plosky Tolbachik Volcano, Kamchatka. *Journal of Volcanology and Geothermal Research*, *307*, 98–106. https://doi.org/10.1016/j.jvolgeores.2015.07.010

U.S. Standard Atmosphere. (1976). U.S. Government Printing Office. Retrieve from https://www.google.com/url?sa=t&rct=j&q=&esrc=s&source=web&cd=&ved=2ahUKEwjkk67Yivn7AhW5TWwGHSb-BU4QFnoECA8QAQ&url=https%3A%2F%2Fwww.ngdc.noaa.gov%2Fstp%2Fspace-weather%2Fonline-publications%2Fmiscellaneous%2Fus-standard-atmosphere-1976%2Fus-standard-atmosphere_st76-1562_noaa.pdf&usg=AOvVaw2PxOPdTVKXBXOVW5M_hQEc

VanderPlas, J. T. (2018). Understanding the Lomb-Scargle periodogram. *The Astrophysical Journal—Supplement Series*, *236*(1), 16. https://doi.org/10.3847/1538-4365/aab766

Velasquez, G., Arellano, S., Bucarey, C., & Galle, B. (2020a). SO_2 flux of COPAHUE Volcano (Version 1) [Dataset]. NOVAC Database. https://doi.org/10.17196/NOVAC.COPAHUE.001

Velasquez, G., Arellano, S., Bucarey, C., Hansteen, T., Bredemeyer, S., & Galle, B. (2020b). SO_2 flux of VILLARRICA Volcano (Version 1) [Dataset]. NOVAC Database. https://doi.org/10.17196/NOVAC.VILLARRICA.001

Vita, F., Arellano, S., Inguaggiato, S., & Galle, B. (2020). SO_2 flux of VULCANO Volcano (Version 1) [Dataset]. NOVAC Database. https://doi.org/10.17196/NOVAC.VULCANO.001

Viveiros, F., Ferreira, T., Cabral Vieira, J., Silva, C., & Gaspar, J. L. (2008). Environmental influences on soil CO_2 degassing at Furnas and Fogo volcanoes (São Miguel Island, Azores archipelago). *Journal of Volcanology and Geothermal Research*, *177*(4), 883–893. https://doi.org/10.1016/j.jvolgeores.2008.07.005

Viveiros, F., Ferreira, T., Silva, C., Vieira, J. C., Gaspar, J. L., Virgili, G., & Amaral, P. (2015). Permanent monitoring of soil CO2 degassing at Furnas and Fogo volcanoes (São Miguel Island, Azores). In J. L. Gaspar, J. E. Guest, A. M. Duncan, F. J. A. S. Barriga, & D. K. Chester (Eds.), *Volcanic Geology of São Miguel Island (Azores Archipelago), Geological Society of London, Memoirs* (Vol. 44, pp. 271–288). Geological Society of London. https://doi.org/10.1144/M44.20

Voight, B., Hoblitt, R. P., Clarke, A. B., Lockhart, A. B., Miller, A. D., Lynch, L., & McMahon, J. (1998). Remarkable cyclic ground deformation monitored in real-time on Montserrat, and its use in eruption forecasting. *Geophysical Research Letters*, *25*(18), 3405–3408. https://doi.org/10.1029/98GL01160

Wang, S., Zhang, M., Sun, M., Wang, B., Huang, X., Wang, Q., & Feng, F. (2015). Comparison of surface air temperature derived from NCEP/DOE R2, ERA-Interim, and observations in the arid northwestern China: A consideration of altitude errors. *Theoretical and Applied Climatology*, *119*(1–2), 99–111. https://doi.org/10.1007/s00704-014-1107-1

Warnach, S., Bobrowski, N., Hidalgo, S., Arellano, S., Sihler, H., Dinger, F., et al. (2019). Variation of the BrO/SO_2 molar ratio in the plume of Tungurahua Volcano between 2007 and 2017 and its relationship to volcanic activity. *Frontiers of Earth Science*, *7*, 132. https://doi.org/10.3389/feart.2019.00132

Williams-Jones, G., Stix, J., Heiligmann, M., Barquero, J., Fernandez, E., & Gonzalez, E. D. (2001). A model of degassing and seismicity at Arenal Volcano, Costa Rica. *Journal of Volcanology and Geothermal Research*, *108*(1–4), 121–139. https://doi.org/10.1016/S0377-0273(00)00281-X

Yalire, M., Arellano, S., Kasareka, M., Karume, K., & Galle, B. (2020). SO_2 flux of NYIRAGONGO Volcano (Version 1) [Dataset]. NOVAC Database. https://doi.org/10.17196/NOVAC.NYIRAGONGO.001

Yokoo, A., Iguchi, M., Tameguri, T., & Yamamoto, K. (2013). Processes prior to outbursts of vulcanian eruption at Showa Crater of Sakurajima Volcano. *Bulletin of the Volcanological Society of Japan*, *58*, 163–181.

21699356, 2022, 12, Downloaded from https://agupubs.onlinelibrary.wiley.com/doi/10.1029/2022JB025380 by Cochrane France, Wiley Online Library on [05/01/2023]. See the Terms and Conditions (https://onlinelibrary.wiley.com/terms-and-conditions) on Wiley Online Library for rules of use; OA articles are governed by the applicable Creative Commons License